

1 **Title page**

2

3 **Title**

4 **naRNA is a canonical neutrophil extracellular trap (NET) component**  
5 **and novel inflammation-amplifying composite DAMP**

6

7 **Running title**

8 naRNA – canonical NET component and composite DAMP

9 **Authors**

10 Francesca Bork<sup>1</sup>, Carsten L. Greve<sup>1</sup>, Christine Youn<sup>2</sup>, Sirui Chen<sup>1</sup>, Yu Wang<sup>2</sup>, Masoud Nasri<sup>3</sup>, Jule  
11 Focken<sup>4</sup>, Jasmin Scheurer<sup>4</sup>, Pujan Engels<sup>1</sup>, Marissa Dubbelaar<sup>1,5</sup>, Katharina Hipp<sup>6</sup>, Birgit Schitteck<sup>4,7,8</sup>,  
12 Stefanie Bugl<sup>1</sup>, Markus W. Löffler<sup>1,7,9</sup>, Julia Skokowa<sup>3,7</sup>, Nathan K. Archer<sup>2</sup> (ORCID: 0000-0002-8212-  
13 8985), Alexander N.R. Weber<sup>1,7,8\*</sup> (ORCID: 0000-0002-8627-7056)

14 **Author information**

15 <sup>1</sup>Interfaculty Institute for Cell Biology, Department of Immunology, University of Tübingen, Auf der  
16 Morgenstelle 15, 72076 Tübingen, Germany

17 <sup>2</sup>Department of Dermatology, Johns Hopkins University School of Medicine, Baltimore, MD 21231,  
18 USA

19 <sup>3</sup>Division of Translational Oncology, Department of Oncology, Hematology, Clinical Immunology and  
20 Rheumatology, University Hospital Tübingen, Otfried-Müller Str. 10, 72076 Tübingen, Germany

21 <sup>4</sup>Division of Dermatooncology, Department of Dermatology, University Hospital Tübingen,  
22 Liebermeisterstr. 25, 72076 Tübingen, Germany

23 <sup>5</sup>Quantitative Biology Center (QBiC), University of Tübingen, Auf der Morgenstelle 10, 72076  
24 Tübingen, Germany

25 <sup>6</sup>Electron Microscopy Facility, Max Planck Institute for Biology Tübingen, Max-Planck-Ring 5, 72076  
26 Tübingen, Germany

27 <sup>7</sup>iFIT – Cluster of Excellence (EXC 2180) "Image-Guided and Functionally Instructed Tumor Therapies",  
28 University of Tübingen, Germany

29 <sup>8</sup>CMFI – Cluster of Excellence (EXC 2124) "Controlling microbes to fight infection", University of  
30 Tübingen, Germany.

31 <sup>9</sup>Department of General, Visceral and Transplant Surgery, University Hospital Tübingen, Hoppe-  
32 Seyler-Str. 3, 72076 Tübingen, Germany and Department of Clinical Pharmacology, University  
33 Hospital Tübingen, Auf der Morgenstelle 8, 72076 Tübingen, Germany

34

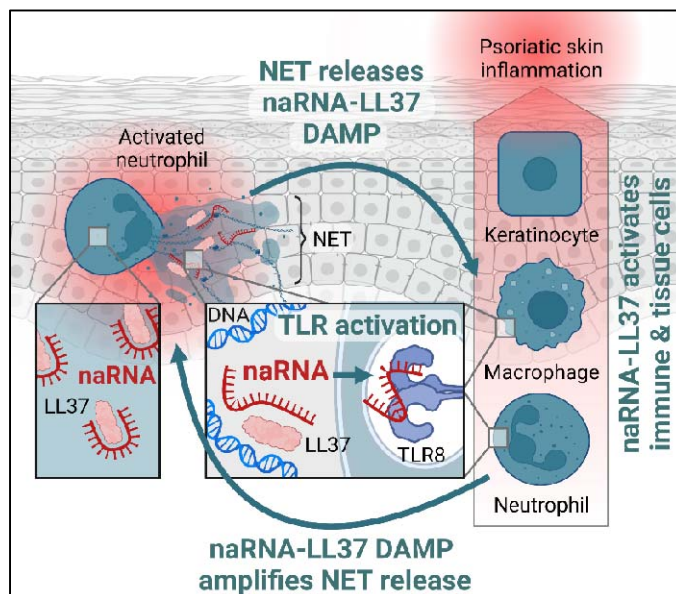
35 **Corresponding Author**

36 Alexander N. R. Weber, Interfaculty Institute for Cell Biology, Department of Immunology, University  
37 of Tübingen, Auf der Morgenstelle 15, 72076 Tübingen, Germany. Tel.: +49 7071 29 87623. Fax: +49  
38 7071 29 4579. Email: [alexander.weber@uni-tuebingen.de](mailto:alexander.weber@uni-tuebingen.de); ORCID: 0000-0002-8627-7056, Twitter  
39 @aweberlab

40 **Abstract**

41 Neutrophil extracellular traps (NETs) have emerged as a key feature of cellular innate immunity  
42 mediated by polymorphonuclear neutrophils (PMNs), the primary leukocyte population in humans.  
43 Forming web-like structures composed of DNA, histones, and antimicrobial proteins, NETs trap and  
44 kill microbial invaders and thus enhance host defense. However, they have also been linked to  
45 inflammatory states, e.g. in atherosclerosis or psoriasis. Whilst DNA has been in focus as a primary  
46 structural component of NETs, we here characterize naRNA (NET-associated RNA), as a new  
47 canonical, abundant, and largely unexplored NET component. naRNA decorated all types of NETs in  
48 complex with the antimicrobial peptide LL37. In fact, naRNA was pre-associated with LL37  
49 intracellularly as a 'composite' danger-associated molecular pattern (DAMP) prior to neutrophil  
50 activation. Externalized, naRNA propagated NET formation in naïve PMN, dependent on TLR8 in  
51 humans and Tlr13 in mice, in vitro and in vivo. naRNA-TLR8/Tlr13 signaling contributed significantly  
52 to the highly sensitive pro-inflammatory response of both tissue cells, like keratinocytes, and other  
53 immune cell types, such as macrophages. Those responses could be blocked by inhibition and genetic  
54 ablation of RNA receptors or RNase treatment. Importantly, in vivo naRNA strongly drove skin  
55 inflammation whereas genetic ablation of RNA sensing drastically ameliorated skin inflammation in  
56 the imiquimod psoriasis model. Our data highlight naRNA as a novel composite DAMP signaling and  
57 amplifying neutrophil activation. Moreover, naRNA emerges as the likely driver of inflammation in  
58 conditions previously linked to NETs and extracellular RNA, suggesting blockade of TLR-mediated  
59 RNA sensing as potential new intervention target.

60 **Graphical abstract**



61

62 Created

with

biorender.com

## 63 **Introduction**

64 The formation of Neutrophil Extracellular Traps (NETs), since its discovery in 2004 (Brinkmann,  
65 Reichard et al. 2004), has emerged as a fascinating phenomenon of host defense. Hereby  
66 neutrophils, the primary leukocyte population, extrude their genomic DNA to form web-like  
67 structures that, similar to barbed wire roadblocks, trap and kill microbial invaders such as bacteria or  
68 fungi (Kruger, Saffarzadeh et al. 2015). DNA is thus a defining structural and functional feature of  
69 NETs. Additionally, DNA-associated proteins, histones and HMGB-1, antimicrobial peptides like LL37  
70 and enzymes such as myeloperoxidase (MPO) are released during the formation of NETs and  
71 contribute to their antimicrobial function (Kruger, Saffarzadeh et al. 2015). More than 1,000  
72 publications on NETs have sought to detail the multi-faceted phenomenon and the processes that  
73 lead to its execution (Boeltz, Amini et al. 2019). However, with the main focus devoted to DNA and  
74 protein components, another primary cellular biomolecule, RNA, has so far received very little  
75 attention in vertebrates. Interestingly, a study in insects showed that, hemocytes (macrophage-like  
76 immune cells) can release both DNA and RNA in NET-like structures during microbe-triggered clotting  
77 reactions, and in response to extracellular RNA or DNA (Altincicek, Stotzel et al. 2008). Our lab  
78 recently provided evidence of a responsiveness of human polymorphonuclear neutrophils (PMNs) to  
79 RNA, but not DNA, in combination with the antimicrobial peptide LL37, fueling neutrophil activation  
80 (Herster, Bittner et al. 2020). In addition, earlier work described a role for DNA- and RNA-LL37  
81 complexes in the activation of plasmacytoid dendritic cells (Lande, Gregorio et al. 2007, Ganguly,  
82 Chamilos et al. 2009). This has given rise to the notion that under certain conditions tolerance to self-  
83 DNA and RNA can be broken involving the nucleic acid-sensing TLR7, TLR8 (ssRNA) and TLR9 (DNA) in  
84 humans and Tlr7, Tlr13 and Tlr9 in mice. In general, many roles have been ascribed to so-called  
85 extracellular RNA (exRNA), for example, macrophage polarization, recruitment of leukocytes to the  
86 site of inflammation, leukocyte rolling at the vascular endothelium, as well as integrin-mediated firm  
87 adhesion of immune cells and promotion of thrombosis (Preissner, Fischer et al. 2020). Additionally,  
88 exRNA is considered as a reliable biomarker for various diseases such as cancer or cardiovascular  
89 pathologies (Schmidt, Engel et al. 2005, Zerneck and Preissner 2016). However, RNA being  
90 considered a short-lived biomolecule, physiological sources of exRNA have been somewhat unclear.  
91 Under sterile conditions, vascular injury, tissue damage, or ischemia have been suggested to trigger  
92 release of exRNA along with other cellular material (Preissner, Fischer et al. 2020). However, it  
93 remains unclear whether these relatively slow processes could amount to physiologically detectable  
94 exRNA amounts in the serum of patients, or whether a rapid, as-yet unidentified process of RNA  
95 extrusion would have to be postulated.

96 We speculated that RNA contained in NETs, so-called NET-associated RNA or naRNA, might lead to a  
97 feed-forward loop of rapidly expanding NET release amongst neutrophils which might also engulf  
98 additional tissue or immune cells able to respond to exRNA. We show here that naRNA drives such a  
99 self-amplifying loop not only engaging PMN but also macrophages, and keratinocytes. naRNA  
100 responsiveness was dependent on *TLR8* and *Tlr13* in human and murine myeloid immune cells,  
101 respectively. Interestingly, naRNA appears pre-complexed to LL37 as a novel composite DAMP.  
102 Notably, in mice naRNA caused considerable skin inflammation in a Tlr13-dependent manner.  
103 Additionally, in a well-established model of psoriatic skin inflammation, genetic ablation of RNA  
104 sensing strongly ameliorated skin inflammation, highlighting naRNA as a potent damage associate  
105 molecular pattern (DAMP) amplifying PMN activation and alerting tissue and other immune cells.

## 106 **Results**

### 107 **naRNA is a common component of NETs**

108 To first identify whether naRNA was a common component of NETs, we compared NETs from human  
109 PMN formed in response to the well-defined molecular agonists PMA, different complexes of LL37  
110 with purified RNA (synthetic, as well as total fungal and bacterial RNA from *S. aureus* and *C. albicans*,  
111 respectively), nigericin (Munzer, Negro et al. 2021) and the live pathogen *C. albicans*. Confocal  
112 microscopy analysis using the well-characterized rRNA-specific antibody, Y10b (Lerner, Lerner et al.  
113 1981), revealed the presence of RNA in all corresponding NETs, independent of stimulus and whether  
114 NET formation was suicidal or not (Fig. 1A, quantified in B; control in Fig. S1A): the RNA signal was  
115 readily detectable along the web-like DNA threads in human NETs. Similar results were obtained in  
116 NETs released by murine bone marrow-derived PMN (BM-PMN, Fig. 1C; control Fig. S1B). To avoid  
117 the use of staining reagents, we also metabolically labeled primary human hematopoietic stem cells  
118 (HSCs) with 5-ethynyluridine (5-EU), a nucleotide that can be incorporated in cellular RNA but not  
119 DNA, and that is amenable to labeling by click chemistry (Presolski, Hong et al. 2011). These HSCs  
120 were then differentiated to neutrophils (Sioud 2020) and the differentiation validated by microscopy  
121 and flow cytometric analysis (Fig. S1C, D). NETs released from HSC-derived PMN could indeed be  
122 labeled with click reagents conferring a fluorescent label only when grown in 5-EU-containing  
123 medium (Fig. 1D). Moreover, the overlap between click-label and rRNA confirmed the specificity of  
124 the staining with anti-rRNA antibodies and indicated that naRNA contained rRNA but also other types  
125 of cellular RNAs. This experiment also unequivocally confirmed that upon PMN stimulation, cellular  
126 RNA is turned into a component of the NET, wherein it decorates the fine, web-like DNA structures.  
127 The localization of naRNA on DNA strands was further confirmed by high-resolution fluorescence  
128 microscopy and 3D analysis (AiryScan, Fig. 1E and Supplemental Movie S1) as well as scanning  
129 electron microscopy (SEM, Fig. 1F; controls Fig. S1E). Extraction of naRNA from PMA-induced NETs

130 (Fig. 1G) and subsequent RNA-sequencing analysis confirmed that purified naRNA contained multiple  
131 RNA types, with noticeably more non-ribosomal RNA than the corresponding total cellular RNA of  
132 PMNs (Fig. 1H). Collectively, these results indicate that naRNA is a canonical component of NETs  
133 released upon multiple stimuli from both human and murine neutrophils.

#### 134 **naRNA is a potent DAMP propagating NET formation in primary PMN**

135 A primary function of NETs is host defense by trapping and killing bacteria. Therefore, we first  
136 explored if naRNA participated in this process (Brinkmann, Reichard et al. 2004). However, the  
137 antibacterial effect of NETs on live *Staphylococcus aureus* (evidenced by lower CFUs compared to  
138 resting PMNs) was similar to that of RNase-treated NETs, whereas DNase digestion reduced the drop  
139 in CFU discernibly but non-significantly (Fig. S2A). Consequently, we turned our attention to a  
140 possible role of naRNA as a DAMP, since primary PMN can respond to synthetic RNA-LL37 complexes  
141 with NET formation, and our analysis indicated that NETs also contain LL37 (Herster, Bittner et al.  
142 2020). To prepare a naRNA-containing stimulant, PMA-induced NETs were prepared as described in  
143 Methods and the original stimulus, PMA, removed by extensive washing before harvesting.  
144 Interestingly, these 'PMA NETs', when applied to naïve PMN from another donor, potently induced  
145 new NETs (Fig. 2B, quantified in C, controls in Fig. S2B). Treatment with an RNase inhibitor enhanced  
146 the stimulatory effect of PMA NETs rendering a 1:500 dilution of PMA-NETs more effective than a  
147 1:50 dilution of non-treated PMA-NETs (Fig. 2B, C, controls Fig. S2B). Interestingly, similar NET  
148 preparations from mock-treated PMNs (here referred to as 'mock NETs') did not stimulate NET  
149 formation under the same experimental conditions. To rule out the possibility that residual PMA in  
150 PMA NETs could be responsible for the observed stimulatory effects, RNase treatment was also  
151 performed which strongly reduced NET formation (Fig. 2D, quantified in E; controls Fig. S2C).  
152 Interestingly, DNase digestion had the same effect as RNase treatment, probably because  
153 digestions/removal of the DNA scaffold would cause a loss of associated naRNA (cf. Fig. 1E). This was  
154 also confirmed by rapid loss of the RNA signal (using the RNA-selective dye, SYTO RNAselect (Herster,  
155 Bittner et al. 2020) in time-lapse digestion analysis of DNA digestions (Supplemental Movie S2 and  
156 S3). Bearing in mind that PMNs do not respond to DNA or DNA-LL37 complexes (Herster, Bittner et  
157 al. 2020), the opposing effects of RNase inhibitor and RNase treatments thus clearly indicated naRNA  
158 (and not DNA) to be the relevant immunostimulatory component for NETs to drive the activation of  
159 naïve PMN. In line with our previous work showing that synthetic RNA or LL37 alone cannot trigger  
160 PMN activation (Herster, Bittner et al. 2020), purified 'naked' naRNA isolated from PMA NETs (cf. Fig.  
161 1G) was unable to activate NET formation; however, re-complexing with exogenous LL37 was  
162 sufficient to restore NET formation (Fig. 2F, controls in Fig. S2D). We next investigated whether in  
163 NETs, naRNA co-localized with LL37. Strong co-localization was evident in confocal microscopy  
164 analysis (Fig. 2G) and confirmed by Pearson's colocalization analysis (Fig. 2H). Additional line plot

165 analysis of PMA-stimulated PMN revealed that RNA and LL37 did in fact co-localize in NETs, i.e., after  
166 extrusion (Fig. S2E). Surprisingly, in unstimulated PMNs naRNA and LL37 showed even greater  
167 colocalization (Fig. 2H), suggesting pre-association before extrusion (Fig. S2E). The concept of pre-  
168 packaging also fits with the RNAseq data showing that certain RNA types are lost upon release (*cf.*  
169 Fig. 1H), probably because they are not bound to LL37. Collectively, naRNA appears to be LL37-pre-  
170 associated, and hence a 'composite' DAMP, enabling PMN activation and NET propagation.

### 171 **naRNA DAMP activity is dependent on RNA sensors TLR8/Tlr13**

172 To validate naRNA as an immunostimulatory RNA component from the receptor side, we turned to  
173 HEK293T cells which do not respond to RNA, unless transfected with plasmids encoding the human  
174 ssRNA sensors TLR7 or TLR8 (Colak, Leslie et al. 2014). NF- $\kappa$ B reporter assays revealed that TLR7 or  
175 TLR8- but not TLR9 (a human DNA sensor)-transfected HEK293T cells stimulated with PMA NETs or  
176 mock NETs showed robust NF- $\kappa$ B activity only for PMA NETs (Fig. 3A). R848 (TLR7 and TLR8 agonist)  
177 and TL8 or ssRNA+DOTAP (TLR8 agonist) served as controls. Of note, compared to its cognate agonist  
178 CpG, the DNA sensor TLR9 was only poorly activated by PMA NETs, indicating that naRNA is a  
179 superior immune stimulant compared to NET DNA in this system. Indeed, the observed response of  
180 primary PMNs (Fig. 3B, quantified in C; in Fig. S3A) could be completely blocked by the TLR8-specific  
181 inhibitor, CU-CPT9a (Zhang, Hu et al. 2018), similar to the effects of the PAD4 inhibitor, Cl-amidine  
182 (Fig. 3C and S3A). This revealed the RNA sensor TLR8 (Heil, Hemmi et al. 2004) to be the naRNA  
183 receptor in primary human PMNs. We further genetically validated the involvement of RNA sensing  
184 in naRNA-mediated NET propagation using BM-PMN from *Unc93b1*- or *Tlr13*-defective mice:  
185 whereas in *Unc93b1*-defective mice signaling of all endosomal TLRs is abrogated (Tabeta, Hoebe et  
186 al. 2006), mice lacking *Tlr13*, the murine equivalent of TLR8 (Eigenbrod and Dalpke 2015), specifically  
187 lack ssRNA sensing (Li and Chen 2012), respectively. Confocal microscopy analysis showed that WT  
188 BM-PMN responded readily to both PMA (used as control) and PMA NETs, whereas *Unc93b1* (Fig.  
189 S3B) or *Tlr13* KO PMN (Fig. 3D, quantified in E) only responded to the TLR-independent PMA control  
190 but not PMA NETs. This receptor analysis unequivocally confirmed naRNA to be a primary immune  
191 stimulant in NETs.

### 192 **PMN-derived naRNA triggers broader immune cell and keratinocyte activation**

193 Given the potent effect of naRNA on naïve PMNs (*cf.* Fig. 3B-E) and the ability of human  
194 macrophages to sense RNA via TLR8 (Ishii, Funami et al. 2014), we hypothesized that naRNA might  
195 also directly activate macrophages, which are rapidly recruited at the sites of PMN activation in  
196 peripheral tissues (Mahdavian Delavary, van der Veer et al. 2011), contributing to an inflammatory  
197 process in vivo. We thus assessed the effects of naRNA on genetically modified macrophage-like cell  
198 lines: BlaER1 macrophages (Vierbuchen, Bang et al. 2017) responded to PMA NETs but not mock

199 NETs with IL-8 release, and this was TLR8-dependent as evidenced by comparisons of WT and *TLR8*-  
200 edited BlaER1 cells (Fig. 3F). Use of a naRNA-stabilizing RNase inhibitor during NET preparation (*cf.*  
201 Fig. 2B) drastically increased the potency of PMA NETs on these macrophages. Additionally, TLR8 and  
202 TLR7-edited THP-1 macrophage-like cells (Coch, Hommertgen et al. 2019) responded to PMA NETs  
203 with lower relative IL-8 release than WT THP-1 cells (Fig. S4A), confirming RNA as the active agent in  
204 monocyte/macrophage activation. Human peripheral blood mononuclear cells (PBMCs) were also  
205 stimulated with different NET preparations. RNA-stabilized PMA NETs consistently elicited higher  
206 TNF, IL-6 and IL-8 levels than non-stabilized PMA- or mock NETs (Fig. S4B-D). However, this effect was  
207 not sensitive to the TLR8 inhibitor Cu-CPT9a, which is consistent with the ability of TLR7 to also sense  
208 naRNA (*cf.* Fig. 3A) and possibly due to a mixture of cells being present. Further analysis revealed that  
209 the natural killer (NK) cell line NK-92 MI showed low IFN $\gamma$  release in response to RNA-stabilized PMA  
210 NETs (Fig. S4E). Collectively, our results show that the RNA component of NETs, naRNA, can engage  
211 not only bystander neutrophils in a feed-forward inflammatory response but also other myeloid  
212 (monocytes/macrophages) and lymphoid (NK cells) cellular innate immunity. To investigate whether  
213 non-hematopoietic cells with immune functions, e.g. tissue cells like keratinocytes, could also  
214 respond to RNA-stabilized PMA NETs, N/TERT-1 keratinocytes (Dickson, Hahn et al. 2000) in  
215 monolayers were exposed to PMA-NETs (Fig. 3G). This triggered a dose-dependent IL-8 release  
216 comparable to synthetic RNA+LL37, especially under RNA stabilization by RNase inhibitors. Similar  
217 results were obtained using primary normal human epidermal keratinocyte (NHEK) monolayers (Fig.  
218 3H). Furthermore, in an 'in vivo'-like human skin equivalent 3D model in which natural keratinocyte  
219 differentiation was recapitulated by NHEK cells (Bitschar, Sauer et al. 2019)), PMA but not mock NETs  
220 significantly induced *IL8* mRNA and protein (Fig. 3I, J). Thus, naRNA can not only activate primary  
221 neutrophils in vitro but also trigger broad immune activation in other immune and tissue  
222 cells/equivalents.

### 223 **naRNA displays DAMP activity in vivo in dependence on RNA sensing**

224 Finally, to gain an insight into whether naRNA could trigger inflammation in vivo in an RNA receptor-  
225 dependent manner, we intradermally injected RNase inhibitor-stabilized mock or PMA NETs in the  
226 ears of C57BL6 mice. RNA-stabilized PMA NETs were almost as potent to induce ear swelling as  
227 synthetic RNA+LL37 (Fig. 4A), but even non-stabilized PMA NETs induced a response significantly  
228 higher than mock NETs. The same stimulants were also injected into the ear of *LysM*<sup>EGFP/+</sup> mice, in  
229 which myeloid cells are GFP-positive, thus enabling in vivo monitoring of cellular influx during skin  
230 inflammation. Here, RNA-stabilized PMA NETs elicited even greater cellular influx than synthetic  
231 RNA+LL37 and mock NETs (Fig. 4B). Importantly, a comparison of WT and *Tlr13*-deficient animals  
232 showed that the ear swelling reaction resulting in vivo was naRNA-dependent because RNA-  
233 stabilized PMA-NETs were significantly less effective in *Tlr13*-deficient animals (Fig. 4C).



## 234 **Self-RNA recognition contributes to progressive skin inflammation in experimental psoriasis**

235 Finally, we sought to explore if naRNA was relevant in an animal disease model. The most frequently  
236 used murine model of psoriasis uses the TLR7 ligand imiquimod (IMQ) to trigger increasing skin  
237 inflammation characterized by epidermal thickening and immune cell infiltration. We previously  
238 showed that IMQ treatment also leads to the occurrence of NETs in the tissue (Herster, Bittner et al.  
239 2020). We therefore speculated that naRNA might be involved in disease progression, a hypothesis  
240 that could be probed by genetically ablating naRNA sensing and comparing WT and *Tlr13* KO mice.  
241 Although in the early induction phase, WT and *Tlr13* KO animals showed a similar increase in ear  
242 thickness, the groups diverged from day 3 onwards, after which *Tlr13*-deficient animals were  
243 significantly protected from skin inflammation compared to WT mice (Fig. 4D). The most plausible  
244 explanation is that IMQ-initiated NET formation (Herster, Bittner et al. 2020) amplifies skin  
245 inflammation in WT animals via naRNA, whereas this is prevented in *Tlr13* KO animals. This shows  
246 that naRNA can significantly contribute to inflammation in a well-established disease model and can  
247 act as a potent inflammation-amplifying endogenous DAMP.

## 248 **Discussion**

249 At first sight, it may not seem surprising that the release of NETs, a process that churns up the most  
250 critical compartment of a cell, e.g., the nucleus, also inevitably leads to the release of another  
251 primary cellular biomolecule, namely RNA. However, independently of whether the process is  
252 regulated or not, the release of RNA by NETting PMN appears to have physiological importance as we  
253 have demonstrated here. Rather than acting directly in antimicrobial defense (*cf.* Fig. S2A), naRNA  
254 appears to be an LL37-precomplexed DAMP of PMN origin that can be released in the NETting  
255 process and then activates both PMN and other immune and tissue cells in an RNA sensor-dependent  
256 manner (Fig. S5). Several further findings warrant further discussion:

257 Firstly, our data revise previous concepts of self-RNA and LL37 in the 'breaking' of innate immune  
258 tolerance in psoriasis and the physiological role of NETs in general: We found that only when naRNA  
259 is complexed with LL37, it gains stimulatory properties on neutrophils (*cf.* Fig. 2F), comparable to  
260 other RNAs tested so far. Based on earlier work (Herster, Bittner et al. 2020) (Kulkarni, O'Neill et al.  
261 2021), LL37 thus may function as a physiological 'transfection reagent' of naRNA mediating its uptake  
262 into immune cells, but possibly also shielding it from RNase degradation. LL37 thus moonlights as an  
263 immunomodulatory peptide rather than only possessing antimicrobial activities. However, RNA and  
264 LL37 do not appear to aggregate and co-localize 'accidentally' in NETs: quite unexpectedly, they were  
265 rather found in even greater co-localization in resting neutrophils, indicating a kind of 'pre-  
266 association' and intracellular storage of a pre-defined naRNA-LL37 'composite' DAMP before  
267 extrusion during NET formation. Importantly, the identification of such pre-association challenges

268 existing concepts of LL37-RNA complexes as ‘accidentally assembled’ tolerance breakers in certain  
269 diseases (Ganguly, Chamilos et al. 2009). Rather, it suggests naRNA-LL37 complexes act as  
270 ‘purposefully pre-associated’ DAMPs that arm neutrophils. It will be interesting to study the process  
271 for pre-association for this first ‘composite DAMP’ and elucidate the precise nature of the RNAs  
272 assembled with LL37 in the future. Intracellular (rather than accidental/extracellular) pre-association  
273 points to a specific role of the naRNA-LL37 DAMP in NET biology. Beyond simply amplifying  
274 inflammation, we speculate that the physiological relevance of deploying this composite DAMP upon  
275 NET formation could be to tag fresh NETs with a timed molecular beacon: Freshly extruded NETs  
276 decorated with the naRNA-LL37 DAMP would likely highlight the lingering presence of a pathogenic  
277 microorganism or acute tissue damage to other cells not directly engaged by the threat. The naRNA-  
278 LL37 DAMP would thus label ‘fresh NETs’ as ‘requiring attention’ and triggering further immune  
279 activation. Over time, whilst the DNA-related structural and antimicrobial properties of NETs may  
280 remain longer, inevitable RNA degradation would lead to deactivation of the composite DAMP,  
281 rendering ‘old NETs’ less immunostimulatory. Further work outside the scope of the present study  
282 may explore such a role of naRNA as time-restricted molecular label for NETs.

283 Moreover, our data pertain to the origin and effects of ‘extracellular RNA’ (exRNA). exRNA is a  
284 generic term to indicate a heterogeneous group of RNA molecules which are actively or passively  
285 released during sterile inflammation or infectious processes. exRNA can be released in a ‘free’ state,  
286 bound to proteins or phospholipids, in association with extracellular vesicles (EVs) or apoptotic  
287 bodies (Preissner, Fischer et al. 2020). In all these forms exRNA may function as DAMP but also as  
288 e.g., procoagulant or regenerative factor (Preissner, Fischer et al. 2020). Our data identify naRNA as  
289 the first type of exRNA for which a clear physiological origin (NETs) is provided. We speculate that  
290 our findings will help trace multiple descriptions of exRNA on the one side, to neutrophil ETs on the  
291 other. For example, exRNA has emerged as disease-relevant in atherosclerosis, where it was  
292 described to act as a proinflammatory mediator enhancing the recruitment of leukocytes to the site  
293 of atherosclerotic lesions as shown in a mouse model of accelerated atherosclerosis (Simsekylmaz,  
294 Cabrera-Fuentes et al. 2014). At the same time, NETs have been ascribed a role in amplifying sterile  
295 inflammatory responses in an independent mouse model of atherosclerosis by priming macrophages  
296 (Warnatsch, Ioannou et al. 2015). However, never have these two independent strains of research  
297 been connected. By showing NETs to release naRNA, a type of exRNA, our work connects both lines  
298 of enquiry. Likewise, for rheumatoid arthritis (RA), our work makes a plausible link between exRNA in  
299 synovial fluid contributing to joint inflammation (Neumann, Hasseli et al. 2018), the emerging role of  
300 NETs in RA (Song, Ye et al. 2020) and even a hitherto enigmatic but therapeutically relevant role of  
301 TLR8 (Sacre, Lo et al. 2008, Sacre, Lo et al. 2016). We suspect similar links to emerge for  
302 cardiovascular diseases and cancer if the role of naRNA is thoroughly assessed. Furthermore, the

303 broad sensitivity of immune and tissue cells to naRNA observed by us makes sense of how exRNA  
304 may act pathophysiologically.

305 Although we believe PMN to be the primary trap forming human leukocyte population and hence  
306 naRNA the most significant “trap-associated RNA”, it will be interesting to explore whether mast cell  
307 (MCETs) (Mollerherm, von Kockritz-Blickwede et al. 2016) or macrophage extracellular traps (METs)  
308 (Doster, Rogers et al. 2018) contain RNA. However, unlike PMN, the latter immune cells are not  
309 primary sources of LL37 (Sorensen, Arnljots et al. 1997), so that RNA associated with MCETs or METs  
310 would be of lesser physiological relevance as a DAMP than naRNA due to a lack of LL37. Therefore,  
311 translational approaches, e.g. to restrict trap-RNA mediated amplification of inflammation, should  
312 probably center on PMN-derived naRNA. The use of PAD4 inhibitors has already been investigated in  
313 animal models to treat cancer or atherosclerotic lesions (Li, Lin et al. 2020) (Knight, Luo et al. 2014)  
314 and would represent one potential way of eliminating NETs and hence naRNA-mediated  
315 inflammation. However, this would also prevent the effects of NETs that are beneficial for host  
316 defense (e.g. physical trapping via DNA and antimicrobial enzymatic activities) and may render  
317 treated patients vulnerable to infections. From a translational perspective, our in vivo data indicate  
318 that blockade of RNA sensing might be more advantageous, restricting only naRNA mediated  
319 responses. Although probably not applicable to patients, it is underscored by evidence that  
320 neuroinflammation upon subarachnoid hemorrhage, which is characterized by a NET pathology, is  
321 strongly ameliorated by RNase treatment in vivo (Fruh, Tielking et al. 2021). More applicable to  
322 patients may be the targeting of TLR8 by small molecular antagonists (Vlach, Bender et al. 2021) or  
323 inhibitory oligonucleotides, which are able to block PMN responsiveness to synthetic RNA in vitro  
324 (Herster, Bittner et al. 2020). Exciting is thus the observed efficacy of TLR inhibitory  
325 oligoribonucleotides in a psoriasis mouse model (Jiang, Zhu et al. 2013) and even a first clinical trial in  
326 psoriasis patients (Balak, van Doorn et al. 2017). We could imagine the blockade of naRNA effects via  
327 TLRs highlighted here to emerge as an effective novel strategy to target multiple exRNA or NET-  
328 related inflammatory responses.

## 329 **Figure legends**

### 330 **Fig. 1: naRNA is a canonical component of NETs.**

331 **(A, B)** Confocal microscopy of primary human PMNs stimulated as indicated for 3 h and stained for  
332 naRNA (anti-rRNA Y10b, magenta) and DNA (Hoechst 33342, white;  $n = 3$ , scale bar: 10  $\mu\text{m}$ ,  
333 arrowheads point to selected NET strands; representative images in **A**) were quantified in **B** (each dot  
334 represents one image,  $*p < 0.05$  according to one-way ANOVA). **(C)** Confocal microscopy of primary  
335 murine BM-PMNs stimulated as indicated for 16 h and stained as in **A** ( $n = 3$ , representative images,  
336 scale bar: 10  $\mu\text{m}$ ). **(D)** Confocal microscopy of primary human stem cells differentiated *in vitro*  
337 with/without 100  $\mu\text{M}$  5-ethynyl uridine (5-EU), click-labeled with a fluorescent dye (yellow, total  
338 RNA), anti-rRNA and Hoechst 33342 as in **A** ( $n = 3$ , representative images, scale bar: 10  $\mu\text{m}$ , 2  $\mu\text{m}$  in  
339 cropped image). **(E)** as in **A** but showing 3D image reconstruction of z-stacks ( $n = 3$ , representative  
340 images, scale bar: 10  $\mu\text{m}$ ). **(F)** Scanning electron microscopy of human primary PMNs treated as  
341 indicated and using anti-rRNA primary and immunogold (white arrow)-labeled secondary antibodies  
342 and silver enhancement ( $n = 3$ , representative images, scale bars as indicated; the two rightmost  
343 images show composite images with signals from secondary electron and backscattered electron  
344 detectors for topography and additional material information, respectively). **(G)** Agilent TapeStation  
345 quantification of naRNA isolated from mock or PMA NETs (from  $n = 4-6$  donors, combined data,  
346 mean+SD, each dot represents one biological replicate/donor,  $*p < 0.05$  according to Mann-Whitney  
347 test). **(H)** RNAseq of PMA NET naRNA ( $n = 4$ ) and whole PMN RNA ( $n = 1$ ) (combined data).

### 348 **Fig. 2. naRNA is a DAMP driving NET propagation in human PMN**

349 **(A)** Workflow for NET content preparation from one donor and transfer to naïve human primary  
350 PMN from a second donor. **(B)** Confocal microscopy of primary human PMNs stimulated with NET  
351 content harvested with/without RNase inhibitor and diluted 1:50 or 1:500, and then stained for  
352 NETs/DNA (Hoechst 33342,  $n = 9$ , representative images, scale bar: 10  $\mu\text{m}$ ). **(C)** Quantification of **B**  
353 using DNA (Hoechst 33342) signal to quantify NET formation ( $n = 3$ , combined data, mean+SD, each  
354 dot represents one image,  $*p < 0.05$  according to one-way ANOVA). **(D)** as in **B** but with/without pre-  
355 digestion of NET content with RNase A or DNase I ( $n = 3$ , representative images; scale bar: 10  $\mu\text{m}$ ). **(E)**  
356 Quantification of **D** ( $n = 3$ , combined data, mean+SD, each dot represents the number of NET-positive  
357 tiles in one image quantified from three images/condition,  $*p < 0.05$  according to one-way ANOVA).  
358 **(F)** As in **B** but using purified naRNA (*cf.* Fig. 1G) alone or in complex with exogenously added LL37 ( $n$   
359 = 3, representative images; scale bar: 10  $\mu\text{m}$ ). **(G)** Confocal microscopy of primary human PMNs  
360 stimulated as indicated for 3 h and stained for naRNA (anti-rRNA Y10b, magenta), LL37 (anti-hLL37-  
361 DyLight550, yellow), and DNA (Hoechst 33342, white;  $n = 3$ , representative images, scale bar 10  $\mu\text{m}$ ).

362 (H) Pearson's correlation coefficient (colocalization) analysis of G (n = 3, combined data, mean+SD,  
363 each dot represents one image, three images/condition, \*p<0.05 according to one-way ANOVA).

364 **Fig. 3. naRNA activity depends on RNA sensors**

365 (A) NF- $\kappa$ B dual luciferase assay in HEK293T cell transiently transfected and stimulated as indicated  
366 (eV = empty vector, n=3-5, combined data, mean+SD, \*p<0.05 according to one-way ANOVA). (B)  
367 Confocal microscopy of human primary PMNs stimulated as indicated in the presence or absence of  
368 CU-CPT9a (100 nM) or Cl-amidine (200  $\mu$ M, not shown) and stained for NETs/DNA (Hoechst 33342,  
369 white, n = 3, representative images, scale bar: 10  $\mu$ m). (C) Quantification of B using DNA (Hoechst  
370 33342) signal to quantify NET formation (n = 3, combined data, mean+SD, each dot represents the  
371 number of NET-positive tiles in one image, three images/condition, \*p<0.05 according to non-  
372 parametric one-way ANOVA). (D) Confocal microscopy analysis of primary C57BL/6 WT or *Tlr13*<sup>-/-</sup>  
373 murine BM-PMNs stimulated as indicated and stained for NETs/DNA (Hoechst 33342, white, n = 3,  
374 representative images, scale bar: 10  $\mu$ m). (E) Quantification of D as in C (n = 3, \*p<0.05 according to  
375 one-way ANOVA. (F) Triplicate IL-8 ELISA from WT, *TLR8*<sup>-/-</sup> and *UNC93B1*<sup>-/-</sup> BlaER1 macrophage-like  
376 cells stimulated as indicated for 18 h (n = 2-3, combined data, mean+SD, each dot represents one  
377 biological replicate, \*p<0.05 according to one-way ANOVA). (G) Triplicate IL-8 ELISA from N/TERT-1  
378 keratinocytes stimulated as indicated for 24 h (n = 3, combined data, mean+SD, each dot represents  
379 one biological replicate, \*p<0.05 according to one-way ANOVA). (H) as in G but with primary normal  
380 human epidermal keratinocytes (NHEK) (n = 3, combined data, mean+SD, each dot represents one  
381 biological replicate, \*p<0.05 according to one-way ANOVA). (I, J) Triplicate relative (to unstimulated)  
382 *IL8* mRNA qPCR or IL-8 ELISA from NHEK 3D human skin equivalent constructs stimulated as indicated  
383 for 24 h (n = 2, representative of one biological replicate is shown, mean+SD, each dot represents  
384 one technical replicate, \*p<0.05 according to one-way ANOVA).

385 **Fig. 4. naRNA is a driver of NET-associated *in vivo* inflammation**

386 (A) Ear thickness quantified daily in WT C57BL6 mice injected intradermally *in vivo* on day 0 as  
387 indicated (n = 5 per group, combined data, mean+SD, \*p<0.05 according to two-way ANOVA). (B)  
388 Fluorescence imaging monitored hourly in *LysM*<sup>EGFP/+</sup> mice injected intradermally *in vivo* at t=0 as  
389 indicated (n = 10 per group, combined data, mean+SD, \*p<0.05 according to two-way ANOVA). (C) As  
390 in A but also using *Tlr13*<sup>-/-</sup> mice (n = 7, combined data, mean+SD, \*p<0.05 according to two-way  
391 ANOVA). (D) As in C but instead of intradermal injection with topical imiquimod application on day 0-  
392 4 (C57BL/6 n = 5, *Tlr13*<sup>-/-</sup> n = 3, combined data, mean+SD, \*p<0.05 according to two-way ANOVA).

393 **Fig. S1. Controls of IF microscopy, stem cell-derived PMNs, and electron microscopy**

394 (A) Confocal microscopy of unstimulated primary human PMNs (control to Fig. 1A) after 3 h and  
395 stained for naRNA (anti-rRNA Y10b, magenta) and DNA (Hoechst 33342, white; n = 3, representative

396 images, scale bar: 10  $\mu$ m). **(B)** Confocal microscopy of unstimulated primary murine BM-PMNs  
397 (control to Fig. 1C) after 16 h and stained as in **A** (n = 3, representative images, scale bar: 10  $\mu$ m). **(C)**  
398 Brightfield microscopy analysis of cytospun control primary human stem cell-derived PMNs (control  
399 to Fig. 1D) differentiated *in vitro* with/without 100  $\mu$ M 5-Ethynyluridine (5-EU, n = 3, representative  
400 images, scale bar: 20  $\mu$ m). **(D)** FACS analysis for cells shown in **C** and Fig. 1D (n=3, representative  
401 data). **(E)** Scanning electron microscopy of PMA-treated human primary PMNs showing only  
402 secondary antibody staining (no primary antibody) control of Fig. 1F (n = 1, representative data; the  
403 image on the right is a composite image with signals from secondary electron and backscattered  
404 electron detectors for topography and additional material information, respectively).

405 **Fig. S2. Antibacterial effect of NETs on live *S. aureus*, controls of IF microscopy and line plot**  
406 **analysis of naRNA and LL37**

407 **(A)** Extracellular bactericidal activity of human PMN/NETs after infection with *S. aureus* and  
408 treatment with RNase A and DNase I during or after formation of PMA-induced NETs (n = 8,  
409 combined data, mean+SD, \*p<0.05 according to one-way ANOVA). **(B)** Confocal microscopy of  
410 unstimulated or PMA-stimulated primary human PMNs (control to Fig. 2B) after 3 h, stained DNA  
411 (Hoechst 33342, white; n = 9, representative images; scale bar: 10  $\mu$ m). **(C)** as in **B** but controls of Fig.  
412 2D (n = 3). **(D)** as in **B** but controls of Fig. 2F (n = 3). **(E)** Confocal microscopy of primary human PMNs  
413 stimulated as indicated for 3 h and stained for naRNA (anti-rRNA Y10b, magenta), LL37 (anti-hLL37-  
414 DyLight550, yellow) and DNA (Hoechst 33342, white; n = 3, representative images, scale bar 10  $\mu$ m).  
415 The line plot analysis of LL37, RNA and DNA staining was performed using ZenBlue3 software (n=2).  
416 Two different line plots from the same representative image are shown.

417 **Fig. S3. Inhibition of PAD4 in human PMNs during NET formation assay and *Unc93b1*<sup>-/-</sup> BM-PMN**  
418 **stimulation with human NETs**

419 **(A)** Confocal microscopy of stimulated primary human PMNs after 3 h and stained for DNA (Hoechst  
420 33342, white) in the presence or absence of the PAD4-inhibitor Cl-amidine (200  $\mu$ M, n = 3,  
421 representative images; scale bar 10  $\mu$ m). **(B)** Confocal microscopy of unstimulated primary C57BL/6  
422 WT or *Unc93b1*<sup>-/-</sup> murine BM-PMNs stimulated as indicated for 16 h as in **A** (n = 3 WT, n = 1 *Unc93b1*<sup>-/-</sup>  
423 <sup>-/-</sup>, representative images, scale bar: 10  $\mu$ m).

424 **Fig. S4. Immune responses of PBMCs, macrophages, and NK-cells to NETs and in vivo fluorescence**  
425 **imaging**

426 **(A)** Triplicate IL-8 ELISA from WT, *TLR8*<sup>-/-</sup> and *TLR7*<sup>-/-</sup> THP-1 cells stimulated as indicated for 18 h,  
427 normalized to PMA+ionomycin control (n = 4, combined data, mean+SD, each dot represents one  
428 biological replicate, \*p<0.05 according to one-way ANOVA). **(B-D)** Triplicate ELISA for TNF (**A**, n = 4),  
429 IL-6 (**B**, n = 3), and IL-8 (**C**, n = 3) from primary human PBMCs stimulated as indicated with/without  
430 CU-CPT9a for 24 h (combined data, mean+SD, each dot represents one biological replicate, \*p<0.05

431 according to one-way ANOVA). (E) Triplicate IFN- $\gamma$  ELISA from NK-92 MI cells stimulated as indicated  
432 for 24 h (n = 3, combined data, mean+SD, each dot represents one biological replicate, \*p<0.05  
433 according to one-way ANOVA).

#### 434 **Fig. S5. Graphical abstract**

#### 435 **Supplemental movie S1: 3D reconstruction of NET DNA network decorated with naRNA**

436 Confocal microscopy of primary human PMNs stimulated with PMA for 3 h, stained for naRNA (anti-  
437 rRNA Y10b, magenta) and DNA (Hoechst 33342, white; n = 3) and 3D analysis and animation were  
438 performed.

#### 439 **Supplemental movie S2: Digest of naRNA in PMA-induced NETs**

440 Confocal live microscopy of RNase digestion of NETs obtained from primary human PMNs stimulated  
441 with PMA for 3 h, stained for naRNA (SYTO RNaselect, magenta) and DNA (Hoechst 33342, white; n =  
442 3). RNase A was added, and live cell imaging was immediately started (n = 3, scale bar 20  $\mu$ m).

#### 443 **Supplemental movie S3: DNase degrades not only DNA but also naRNA in NETs**

444 Confocal live microscopy of DNase digestion of NETs obtained from primary human PMNs stimulated  
445 with PMA for 3 h, stained for naRNA (SYTO RNaselect, magenta) and DNA (Hoechst 33342, white; n =  
446 3). DNase I was added, and live cell imaging was immediately started (n = 3, scale bar 20  $\mu$ m).

447

## 448 **References**

- 449 Altincicek, B., S. Stotzel, M. Wygrecka, K. T. Preissner and A. Vilcinskas (2008). "Host-derived  
450 extracellular nucleic acids enhance innate immune responses, induce coagulation, and prolong  
451 survival upon infection in insects." *J Immunol* **181**(4): 2705-2712.
- 452 Balak, D. M., M. B. van Doorn, R. D. Arbeit, R. Rijneveld, E. Klaassen, T. Sullivan, J. Brevard, H. B. Thio,  
453 E. P. Prens, J. Burggraaf and R. Rissmann (2017). "IMO-8400, a toll-like receptor 7, 8, and 9  
454 antagonist, demonstrates clinical activity in a phase 2a, randomized, placebo-controlled trial in  
455 patients with moderate-to-severe plaque psoriasis." *Clin Immunol* **174**: 63-72.
- 456 Bitschar, K., B. Sauer, J. Focken, H. Dehmer, S. Moos, M. Konnerth, N. A. Schilling, S. Grond, H.  
457 Kalbacher, F. C. Kurschus, F. Gotz, B. Krismer, A. Peschel and B. Schitteck (2019). "Lugdunin amplifies  
458 innate immune responses in the skin in synergy with host- and microbiota-derived factors." *Nat*  
459 *Commun* **10**(1): 2730.
- 460 Bitschar, K., L. Staudenmaier, L. Klink, J. Focken, B. Sauer, B. Fehrenbacher, F. Herster, Z. Bittner, L.  
461 Bleul, M. Schaller, C. Wolz, A. N. R. Weber, A. Peschel and B. Schitteck (2020). "Staphylococcus aureus  
462 Skin Colonization Is Enhanced by the Interaction of Neutrophil Extracellular Traps with  
463 Keratinocytes." *J Invest Dermatol* **140**(5): 1054-1065 e1054.
- 464 Boeltz, S., P. Amini, H. J. Anders, F. Andrade, R. Bilyy, S. Chatfield, I. Cichon, D. M. Clancy, J. Desai, T.  
465 Dumych, N. Dwivedi, R. A. Gordon, J. Hahn, A. Hidalgo, M. H. Hoffmann, M. J. Kaplan, J. S. Knight, E.  
466 Kolaczowska, P. Kubes, M. Leppkes, A. A. Manfredi, S. J. Martin, C. Maueroeder, N. Maugeri, I.  
467 Mitroulis, L. E. Munoz, D. Nakazawa, I. Neeli, V. Nizet, E. Pieterse, M. Z. Radic, C. Reinwald, K. Ritis, P.  
468 Rovere-Querini, M. Santocki, C. Schauer, G. Schett, M. J. Shlomchik, H. U. Simon, P. Skendros, D.  
469 Stojkov, P. Vandenabeele, T. V. Berghe, J. van der Vlag, L. Vitkov, M. von Kockritz-Blickwede, S.

470 Yousefi, A. Zarbock and M. Herrmann (2019). "To NET or not to NET: current opinions and state of the  
471 science regarding the formation of neutrophil extracellular traps." *Cell Death Differ* **26**(3): 395-408.

472 Brinkmann, V., U. Reichard, C. Goosmann, B. Fauler, Y. Uhlemann, D. S. Weiss, Y. Weinrauch and A.  
473 Zychlinsky (2004). "Neutrophil extracellular traps kill bacteria." *Science* **303**(5663): 1532-1535.

474 Chang, T.-H., Y. C. Gloria, M. J. Hellmann, C. L. Greve, D. L. Roy, T. Roger, L. Kasper, B. Hube, S. Pusch,  
475 N. Gow, M. Sørli, A. Tøndervik, B. M. Moerschbacher and A. N. R. Weber (2022). "Transkingdom  
476 mechanism of MAMP generation by chitotriosidase (CHIT1) feeds oligomeric chitin from fungal  
477 pathogens and allergens into TLR2-mediated innate immune sensing." *bioRxiv*:  
478 2022.2002.2017.479713.

479 Coch, C., B. Hommertgen, T. Zillinger, J. Dassler-Plenker, B. Putschli, M. Nastaly, B. M. Kummerer, J. F.  
480 Scheunemann, B. Schumak, S. Specht, M. Schlee, W. Barchet, A. Hoerauf, E. Bartok and G. Hartmann  
481 (2019). "Human TLR8 Senses RNA From Plasmodium falciparum-Infected Red Blood Cells Which Is  
482 Uniquely Required for the IFN-gamma Response in NK Cells." *Front Immunol* **10**: 371.

483 Colak, E., A. Leslie, K. Zausmer, E. Khatamzas, A. V. Kubarenko, T. Pichulik, S. N. Klimosch, A. Mayer,  
484 O. Siggs, A. Hector, R. Fischer, B. Klessner, A. Rautanen, M. Frank, A. V. Hill, B. Manoury, B. Beutler, D.  
485 Hartl, A. Simmons and A. N. Weber (2014). "RNA and imidazoquinolines are sensed by distinct TLR7/8  
486 ectodomain sites resulting in functionally disparate signaling events." *J Immunol* **192**(12): 5963-5973.

487 Dickson, M. A., W. C. Hahn, Y. Ino, V. Ronfard, J. Y. Wu, R. A. Weinberg, D. N. Louis, F. P. Li and J. G.  
488 Rheinwald (2000). "Human keratinocytes that express hTERT and also bypass a p16(INK4a)-enforced  
489 mechanism that limits life span become immortal yet retain normal growth and differentiation  
490 characteristics." *Mol Cell Biol* **20**(4): 1436-1447.

491 Doster, R. S., L. M. Rogers, J. A. Gaddy and D. M. Aronoff (2018). "Macrophage Extracellular Traps: A  
492 Scoping Review." *J Innate Immun* **10**(1): 3-13.

493 Eigenbrod, T. and A. H. Dalpke (2015). "Bacterial RNA: An Underestimated Stimulus for Innate  
494 Immune Responses." *J Immunol* **195**(2): 411-418.

495 Faust, N., F. Varas, L. M. Kelly, S. Heck and T. Graf (2000). "Insertion of enhanced green fluorescent  
496 protein into the lysozyme gene creates mice with green fluorescent granulocytes and macrophages."  
497 *Blood* **96**(2): 719-726.

498 Fruh, A., K. Tielking, F. Schoknecht, S. Liu, U. C. Schneider, S. Fischer, P. Vajkoczy and R. Xu (2021).  
499 "RNase A Inhibits Formation of Neutrophil Extracellular Traps in Subarachnoid Hemorrhage." *Front*  
500 *Physiol* **12**: 724611.

501 Ganguly, D., G. Chamilos, R. Lande, J. Gregorio, S. Meller, V. Facchinetti, B. Homey, F. J. Barrat, T. Sal  
502 and M. Gilliet (2009). "Self-RNA-antimicrobial peptide complexes activate human dendritic cells  
503 through TLR7 and TLR8." *J Exp Med* **206**(9): 1983-1994.

504 Gilliet, M., C. Conrad, M. Geiges, A. Cozzio, W. Thurlimann, G. Burg, F. O. Nestle and R. Dummer  
505 (2004). "Psoriasis triggered by toll-like receptor 7 agonist imiquimod in the presence of dermal  
506 plasmacytoid dendritic cell precursors." *Arch Dermatol* **140**(12): 1490-1495.

507 Heil, F., H. Hemmi, H. Hochrein, F. Ampenberger, C. Kirschning, S. Akira, G. Lipford, H. Wagner and S.  
508 Bauer (2004). "Species-specific recognition of single-stranded RNA via toll-like receptor 7 and 8."  
509 *Science* **303**(5663): 1526-1529.

510 Herster, F., Z. Bittner, N. K. Archer, S. Dickhofer, D. Eisel, T. Eigenbrod, T. Knorpp, N. Schneiderhan-  
511 Marra, M. W. Loffler, H. Kalbacher, T. Vierbuchen, H. Heine, L. S. Miller, D. Hartl, L. Freund, K.  
512 Schakel, M. Heister, K. Ghoreschi and A. N. R. Weber (2020). "Neutrophil extracellular trap-associated  
513 RNA and LL37 enable self-amplifying inflammation in psoriasis." *Nat Commun* **11**(1): 105.

514 Ishii, N., K. Funami, M. Tatematsu, T. Seya and M. Matsumoto (2014). "Endosomal localization of  
515 TLR8 confers distinctive proteolytic processing on human myeloid cells." *J Immunol* **193**(10): 5118-  
516 5128.

517 Jiang, W., F. G. Zhu, L. Bhagat, D. Yu, J. X. Tang, E. R. Kandimalla, N. La Monica and S. Agrawal (2013).  
518 "A Toll-like receptor 7, 8, and 9 antagonist inhibits Th1 and Th17 responses and inflammasome  
519 activation in a model of IL-23-induced psoriasis." *J Invest Dermatol* **133**(7): 1777-1784.

520 Knight, J. S., W. Luo, A. A. O'Dell, S. Yalavarthi, W. Zhao, V. Subramanian, C. Guo, R. C. Grenn, P. R.  
521 Thompson, D. T. Eitzman and M. J. Kaplan (2014). "Peptidylarginine deiminase inhibition reduces



522 vascular damage and modulates innate immune responses in murine models of atherosclerosis." Circ  
523 Res **114**(6): 947-956.

524 Kruger, P., M. Saffarzadeh, A. N. Weber, N. Rieber, M. Radsak, H. von Bernuth, C. Benarafa, D. Roos,  
525 J. Skokowa and D. Hartl (2015). "Neutrophils: Between host defence, immune modulation, and tissue  
526 injury." PLoS Pathog **11**(3): e1004651.

527 Kulkarni, N. N., A. M. O'Neill, T. Dokoshi, E. W. C. Luo, G. C. L. Wong and R. L. Gallo (2021). "Sequence  
528 determinants in the cathelicidin LL-37 that promote inflammation via presentation of RNA to  
529 scavenger receptors." J Biol Chem **297**(1): 100828.

530 Lande, R., J. Gregorio, V. Facchinetti, B. Chatterjee, Y. H. Wang, B. Homey, W. Cao, Y. H. Wang, B. Su,  
531 F. O. Nestle, T. Zal, I. Mellman, J. M. Schroder, Y. J. Liu and M. Gilliet (2007). "Plasmacytoid dendritic  
532 cells sense self-DNA coupled with antimicrobial peptide." Nature **449**(7162): 564-569.

533 Lerner, E. A., M. R. Lerner, C. A. Janeway, Jr. and J. A. Steitz (1981). "Monoclonal antibodies to nucleic  
534 acid-containing cellular constituents: probes for molecular biology and autoimmune disease." Proc  
535 Natl Acad Sci U S A **78**(5): 2737-2741.

536 Li, M., C. Lin, H. Deng, J. Strnad, L. Bernabei, D. T. Vogl, J. J. Burke and Y. Nefedova (2020). "A Novel  
537 Peptidylarginine Deiminase 4 (PAD4) Inhibitor BMS-P5 Blocks Formation of Neutrophil Extracellular  
538 Traps and Delays Progression of Multiple Myeloma." Mol Cancer Ther **19**(7): 1530-1538.

539 Li, X. D. and Z. J. Chen (2012). "Sequence specific detection of bacterial 23S ribosomal RNA by TLR13." Elife **1**: e00102.

541 Mahdavian Delavary, B., W. M. van der Veer, M. van Egmond, F. B. Niessen and R. H. Beelen (2011).  
542 "Macrophages in skin injury and repair." Immunobiology **216**(7): 753-762.

543 Mollerherm, H., M. von Kockritz-Blickwede and K. Branitzki-Heinemann (2016). "Antimicrobial  
544 Activity of Mast Cells: Role and Relevance of Extracellular DNA Traps." Front Immunol **7**: 265.

545 Munzer, P., R. Negro, S. Fukui, L. di Meglio, K. Aymonnier, L. Chu, D. Cherpokova, S. Gutch, N. Sorvillo,  
546 L. Shi, V. G. Magupalli, A. N. R. Weber, R. E. Scharf, C. M. Waterman, H. Wu and D. D. Wagner (2021).  
547 "NLRP3 Inflammasome Assembly in Neutrophils Is Supported by PAD4 and Promotes NETosis Under  
548 Sterile Conditions." Front Immunol **12**: 683803.

549 Neumann, E., R. Hasseli, U. Lange and U. Muller-Ladner (2018). "The Role of Extracellular Nucleic  
550 Acids in Rheumatoid Arthritis." Curr Pharm Biotechnol **19**(15): 1182-1188.

551 Preissner, K. T., S. Fischer and E. Deindl (2020). "Extracellular RNA as a Versatile DAMP and Alarm  
552 Signal That Influences Leukocyte Recruitment in Inflammation and Infection." Front Cell Dev Biol **8**:  
553 619221.

554 Presolski, S. I., V. P. Hong and M. G. Finn (2011). "Copper-Catalyzed Azide-Alkyne Click Chemistry for  
555 Bioconjugation." Curr Protoc Chem Biol **3**(4): 153-162.

556 Sacre, S., A. Lo, B. Gregory, M. Stephens, G. Chamberlain, P. Stott and F. Brennan (2016).  
557 "Oligodeoxynucleotide inhibition of Toll-like receptors 3, 7, 8, and 9 suppresses cytokine production  
558 in a human rheumatoid arthritis model." Eur J Immunol **46**(3): 772-781.

559 Sacre, S. M., A. Lo, B. Gregory, R. E. Simmonds, L. Williams, M. Feldmann, F. M. Brennan and B. M.  
560 Foxwell (2008). "Inhibitors of TLR8 reduce TNF production from human rheumatoid synovial  
561 membrane cultures." J Immunol **181**(11): 8002-8009.

562 Schmidt, B., E. Engel, T. Carstensen, S. Weickmann, M. John, C. Witt and M. Fleischhacker (2005).  
563 "Quantification of free RNA in serum and bronchial lavage: a new diagnostic tool in lung cancer  
564 detection?" Lung Cancer **48**(1): 145-147.

565 Simsekylmaz, S., H. A. Cabrera-Fuentes, S. Meiler, S. Kostin, Y. Baumer, E. A. Liehn, C. Weber, W. A.  
566 Boisvert, K. T. Preissner and A. Zernecke (2014). "Role of extracellular RNA in atherosclerotic plaque  
567 formation in mice." Circulation **129**(5): 598-606.

568 Sioud, M. (2020). "RNA Interference and CRISPR Technologies Technical Advances and New  
569 Therapeutic Opportunities Preface." Rna Interference and Crispr Technologies: Technical Advances  
570 and New Therapeutic Opportunities **2115**: V-Vii.

571 Song, W., J. Ye, N. Pan, C. Tan and M. Herrmann (2020). "Neutrophil Extracellular Traps Tied to  
572 Rheumatoid Arthritis: Points to Ponder." Front Immunol **11**: 578129.

573 Sorensen, O., K. Arnljots, J. B. Cowland, D. F. Bainton and N. Borregaard (1997). "The human  
 574 antibacterial cathelicidin, hCAP-18, is synthesized in myelocytes and metamyelocytes and localized to  
 575 specific granules in neutrophils." *Blood* **90**(7): 2796-2803.  
 576 Tabeta, K., K. Hoebe, E. M. Janssen, X. Du, P. Georgel, K. Crozat, S. Mudd, N. Mann, S. Sovath, J.  
 577 Goode, L. Shamel, A. A. Herskovits, D. A. Portnoy, M. Cooke, L. M. Tarantino, T. Wiltshire, B. E.  
 578 Steinberg, S. Grinstein and B. Beutler (2006). "The Unc93b1 mutation 3d disrupts exogenous antigen  
 579 presentation and signaling via Toll-like receptors 3, 7 and 9." *Nat Immunol* **7**(2): 156-164.  
 580 Vierbuchen, T., C. Bang, H. Rosigkeit, R. A. Schmitz and H. Heine (2017). "The Human-Associated  
 581 Archaeon *Methanosphaera stadtmanae* Is Recognized through Its RNA and Induces TLR8-Dependent  
 582 NLRP3 Inflammasome Activation." *Front Immunol* **8**: 1535.  
 583 Vlach, J., A. T. Bender, M. Przetak, A. Pereira, A. Deshpande, T. L. Johnson, S. Reissig, E. Tzvetkov, D.  
 584 Musil, N. T. Morse, P. Haselmayer, S. C. Zimmerli, S. L. Okitsu, R. L. Walsky and B. Sherer (2021).  
 585 "Discovery of M5049: A Novel Selective Toll-Like Receptor 7/8 Inhibitor for Treatment of  
 586 Autoimmunity." *J Pharmacol Exp Ther* **376**(3): 397-409.  
 587 Warnatsch, A., M. Ioannou, Q. Wang and V. Papayannopoulos (2015). "Inflammation. Neutrophil  
 588 extracellular traps license macrophages for cytokine production in atherosclerosis." *Science*  
 589 **349**(6245): 316-320.  
 590 Zack, G. W., W. E. Rogers and S. A. Latt (1977). "Automatic-Measurement of Sister Chromatid  
 591 Exchange Frequency." *Journal of Histochemistry & Cytochemistry* **25**(7): 741-753.  
 592 Zernecke, A. and K. T. Preissner (2016). "Extracellular Ribonucleic Acids (RNA) Enter the Stage in  
 593 Cardiovascular Disease." *Circ Res* **118**(3): 469-479.  
 594 Zhang, S., Z. Hu, H. Tanji, S. Jiang, N. Das, J. Li, K. Sakaniwa, J. Jin, Y. Bian, U. Ohto, T. Shimizu and H.  
 595 Yin (2018). "Small-molecule inhibition of TLR8 through stabilization of its resting state." *Nat Chem*  
 596 *Biol* **14**(1): 58-64.  
 597

598 **Additional information**

599 **Author contributions:** according to Credit guidelines:

	FB	CGL	CY	SC	YW	MN	JF	JS	PE	MD	KH	BS	MWL	YS	NKA
Conceptualization	x														
Data curation															
Formal analysis	x	x	x	x		x	x	x	x		x				x
Funding acquisition												x			
Investigation	x	x	x	x		x	x	x	x	x	X				
Methodology											X			x	
Project administration					x								X		
Resources													X		
Software															
Supervision	X											x		x	x
Validation	X														x
Visualization	x	x	x								X				
Writing: original draft	x														
Writing: review and editing	x	x	x	x	x	x	x	x	x	x	x	x	x	x	x

600

601 **Conflict of interest statement**

602 NKA has received previous grant support from Pfizer and Boehringer Ingelheim and was a paid  
 603 consultant for Janssen Pharmaceuticals. All other authors declare no competing interests. S.D.G.

## 604 **Acknowledgments**

605 We gratefully acknowledge Jim Rheinwald, Holger Heine, Austin Chang, Thomas Zillinger for the  
606 provision of reagents, respectively, and Jon Kagan and Libera Lo Presti for helpful scientific and  
607 editorial comments. We thank all voluntary healthy donors of biomaterials for participating in the  
608 study. The study was supported by the Deutsche Forschungsgemeinschaft (German Research  
609 Foundation, DFG) grants CRC TR156 “The skin as an immune sensor and effector organ –  
610 Orchestrating local and systemic immunity” (to FB, CG, JF, JS, BS and ANRW), NIH grants  
611 R01AI146177, R01AR073665, and R01AR069502 (to NKA). NKA. has received previous grant support  
612 from Pfizer and Boehringer Ingelheim and was a paid consultant for Janssen Pharmaceuticals.  
613 Infrastructural funding was provided by the University of Tübingen, the University Hospital Tübingen  
614 and the DFG Clusters of Excellence "iFIT – Image-Guided and Functionally Instructed Tumor  
615 Therapies" (EXC 2180, to AW, PE, BS and MWL), “CMFI – Controlling Microbes to Fight Infection (EXC  
616 2124 to AW and BS). Gefördert durch die Deutsche Forschungsgemeinschaft (DFG) im Rahmen der  
617 Exzellenzstrategie des Bundes und der Länder - EXC 2180 and EXC 2124. The authors declare no  
618 competing financial interests.

619

## 620 **Abbreviations**

621 AF – Alexa Fluor; bRNA – bacterial ribonucleic acid; DAMP – damage-associated molecular pattern; 5-  
622 EU – 5-Ethynyluridine; FACS – Fluorescence Activated Cell Sorting; fRNA – fungal ribonucleic acid;  
623 HEK – Human embryonic kidney; HMGB-1 – High-Mobility-Group-Protein B1; HSC – hematopoietic  
624 stem cell; IFN – Interferon; IL – Interleukin; KO – knockout; MCET – Mast cell extracellular trap; MET  
625 – Macrophage extracellular trap; MPO – Myeloperoxidase; naRNA – Neutrophil extracellular trap-  
626 associated RNA; NET – Neutrophil extracellular trap; NK – natural killer; PAD4 - Peptidyl arginine  
627 deiminase 4; PBMC - Peripheral Blood Mononuclear Cell; PKC- Protein kinase C; PMN –  
628 Polymorphonuclear leukocytes; RT – room temperature; SEM – scanning electron microscopy; TLR –  
629 Toll-like receptor; TNF – Tumor necrosis factor

## 630 **Materials and Methods**

### 631 **Reagents**

632 PMA (tlrl-pma), Nigericin (tlrl-nig), LL37 (tlrl-l37), as well as the PRR ligands LPS (tlrl-peklps), R848  
633 (tlrl-r848), TL8 (tlrl-tl8506), and the TLR8-inhibitor CU-CPT9a (inh-cc9a) were from Invivogen,  
634 Ionomycin was acquired from Sigma (I0634-1MG). RNase inhibitor (N2615) was from Promega,  
635 RNase A (EN0531), DNase I (EN0521) and DNase inhibitor (EN0521) were from Thermo Fisher. The  
636 PAD4-inhibitor Cl-amidine (506282) was from Merck Millipore. DOTAP (L787.2) was from Roth (see  
637 Supplementary Table S1) and ssRNA40 was from Eurogentec (see Supplementary Table S2). Bacterial  
638 RNA isolated from *S. aureus* was prepared as described (Herster, Bittner et al. 2020). Fungal RNA  
639 from *C. albicans* strain SC5314 was isolated as described below, as well as naRNA isolated from PMA  
640 NETs. For complex formation to stimulate cells in a volume of 500  $\mu$ L, 5.8  $\mu$ M ssRNA40 ( $\sim$  34.4  
641  $\mu$ g/mL), fungal RNA (125 ng/mL), bacterial RNA (10  $\mu$ g/mL) or PMA NET derived naRNA ( $\sim$  600 ng/mL)  
642 was mixed with 10  $\mu$ g LL37 and left for 1 h at room temperature (RT). For a smaller volume of cells,  
643 complexes were used in the according fractional amount. For RNA-only or LL37-only controls, the  
644 same amounts and volumes were used replacing one of the components with sterile, endotoxin-free  
645 H<sub>2</sub>O. For complex formation with DOTAP, the according RNA or CpG was incubated with the  
646 transfection reagent for 10 min at RT prior to stimulation of the cells. NET content for stimulation  
647 was prepared as described below. Antibodies used for fluorescence microscopy, as well as click  
648 chemistry reagents are listed in Supplementary Tables S3 and S4. Constructs used for transfection of  
649 HEK293T cells are listed in Supplementary Table S5.

### 650 **Preparation of fungal RNA from *C. albicans***

651 *C. albicans* SC5314 (kindly cultured and prepared by Tzu-Hsuan Chang, Tübingen) was plated in a  
652 slant tube containing YPD agar and grown overnight at 30 °C as described in (Chang, Gloria et al.  
653 2022). One colony was picked from the slant tube and resuspended in 500  $\mu$ L YPD medium,  
654 centrifuged at 10,000 rpm for 1 min and washed with phosphate-buffered saline (PBS). Afterwards,  
655 the pellet was resuspended in 200  $\mu$ L RLT buffer (derived from RNeasy Mini Kit, Qiagen, #74106) and  
656 transferred into a 2 mL tube containing 0.5 mm diameter ceramic beads. The tube was filled up to 1  
657 mL with RLT buffer and the fungi were subsequently homogenized by using a microtube  
658 homogenizer (BeadBug™, Merck) with an interval of seven times 2 min shaking at 2800 rpm and 1  
659 min cooling break on ice. The supernatant was transferred into a new tube containing 1 mL 75%  
660 ethanol (VWR, 20821.330). The further RNA isolation was performed according to the manufacturer's  
661 instructions using the Qiagen RNeasy Mini Kit for purification of Total RNA from Animal Tissues  
662 (RNeasy Mini Kit, Qiagen, 74106). The RNA was eluted in 30  $\mu$ L RNase DNase-free H<sub>2</sub>O and the  
663 concentration was determined with a Nanodrop Spectrophotometer.

### 664 **Mice**

665 *Unc93b1*<sup>3d/3d</sup> (Tabeta, Hoebe et al. 2006), *Tlr13*<sup>-/-</sup> (Li and Chen 2012) (both kindly provided by Tatjana  
666 Eigenbrod, Heidelberg and on C57BL/6 background) and WT C57BL/6 mice between 8 and 20 weeks  
667 of age were used in accordance with local institutional guidelines on animal experiments, regular  
668 hygiene monitoring, and specific locally approved protocols compliant with the German regulations  
669 of the Gesellschaft für Versuchstierkunde/Society for Laboratory Animal Science (GV-SOLAS) and the  
670 European Health Law of the Federation of Laboratory Animal Science Associations (FELASA) for  
671 sacrificing and *in vivo* work. *Unc93b1*<sup>3d/3d</sup>, *Tlr13*<sup>-/-</sup> and WT C57BL/6 control mice were housed in  
672 controlled specific-pathogen-free animal facilities at the Interfaculty Institute of Cell Biology,  
673 Tübingen. Local federal authority for the approval of experimental protocols was the  
674 Regierungspräsidium Tübingen. LysM<sup>EGFP/+</sup> (Faust, Varas et al. 2000), *Tlr13*<sup>-/-</sup> mice (Li and Chen 2012)  
675 (kindly provided by James Chen, Houston and David Nemazee, La Jolla) and WT (all on a C57BL/6  
676 background) mouse strains were also bred and maintained under the specific pathogen-free  
677 conditions, with air isolated cages at an American Association for the Accreditation of Laboratory

678 Animal Care (AAALAC)-accredited animal facility at Johns Hopkins University and handled according  
679 to procedures described in the Guide for the Care and Use of Laboratory Animals as well as Johns  
680 Hopkins University's policies and procedures as set forth in the Johns Hopkins University Animal Care  
681 and Use Training Manual, and all animal experiments were approved by the Johns Hopkins University  
682 Animal Care and Use Committee (MO21M378). Gender-and age-matched 6-8 week old mice were  
683 used for each experiment.

#### 684 **Isolation and stimulation of primary bone-marrow-derived polymorphonuclear neutrophils (BM- 685 PMNs)**

686 Bone-marrow (BM)-PMNs were isolated from the bone marrow as described (Herster, Bittner et al.  
687 2020). In brief, bones were isolated from the respective mice and the bone marrow was flushed out.  
688 Afterwards, neutrophils were isolated using magnetic separation (mouse Neutrophil isolation kit,  
689 Miltenyi Biotec, 130-097-658) following the manufacturer's instructions. In total,  $1 \times 10^5$  cells/well  
690 PMNs were seeded in a 24-well plate, and stimulation was carried out with PMA (600 nM),  
691 ssRNA+LL37 complex (as previously described), nigericin (50  $\mu$ M), live *C. albicans* (MOI1) or human  
692 NET content (mock control and PMA NETs, 1:50 dilution) for 16 h at 37°C and 5% CO<sub>2</sub>. Subsequently,  
693 cells were stained for immunofluorescence.

#### 694 **Study participants and human blood or tissue sample acquisition**

695 All healthy donors included in this study provided their written informed consent before  
696 participation. Approval for use of biomaterials was obtained for this project by the local ethics  
697 committee of the Medical Faculty Tübingen in accordance with the principles laid down in the  
698 Declaration of Helsinki as well as applicable laws and regulations.

#### 699 **Primary human neutrophil isolation and stimulation**

700 Neutrophils of healthy human donors were isolated as described (Herster, Bittner et al. 2020). In  
701 brief, EDTA-anticoagulated whole blood was diluted in PBS (Thermo Fisher, 14190-169), loaded on  
702 Ficoll (1.077 g/mL, Sigma, 10771) and centrifuged for 25 min at 509 x g at RT without brake.  
703 Afterwards, all layers except the erythrocyte-granulocyte layer were discarded and erythrocyte lysis  
704 was performed twice (for 20 and for 10 min) using 1x ammonium chloride erythrocyte lysis buffer  
705 (see Supplementary Table S6) at 4 °C on roller shaker. The remaining cells were resuspended in  
706 culture medium (RPMI culture medium (Sigma-Aldrich, R8758) + 10% FBS (heat-inactivated, sterile  
707 filtered, Th. Geyer, 11682258)) to a concentration of  $1.6 \times 10^6$  cells/mL. 500  $\mu$ L of cells were seeded  
708 in a 24-well plate for immunofluorescence microscopy or 8 mL of  $5 \times 10^6$  cells/mL in 10 cm uncoated  
709 dishes for NET preparation and naRNA isolation/isolation of whole PMN RNA. After seeding, the cells  
710 were rested for 30 min at 37°C and 5% CO<sub>2</sub>, followed by 3 h stimulation with PMA (600 nM), nigericin  
711 (50  $\mu$ M), live *C. albicans* (MOI2), RNA+LL37 complexes (as previously described) or NET content at  
712 indicated dilutions for IF or 4 h stimulation with PMA (600 nM) for NET preparation. Where indicated,  
713 the cells were incubated with 100 nM TLR8-inhibitor CU-CPT9a or 200  $\mu$ M PAD4-inhibitor Cl-amidine  
714 30 min before stimulation and not replaced during incubation with the respective stimuli.

#### 715 **Primary peripheral blood mononuclear cells (PBMC) isolation and stimulation**

716 PBMCs were isolated from whole blood or buffy coats as described (Herster, Bittner et al. 2020). In  
717 brief, EDTA-anticoagulated blood was diluted in PBS and density gradient separation was performed  
718 as described above. The PBMC layer was then carefully transferred into another reaction tube and  
719 diluted in PBS (1:1). The cell suspension was spun down at 645 x g for 8 min and the cells were  
720 washed two more times in PBS and resuspended in culture medium (RPMI + 10% FBS (heat  
721 inactivated) + 1% L-glutamine) at a density of  $1 \times 10^6$  cells/mL. Afterwards, 200  $\mu$ L of PBMCs were  
722 seeded in a 96-well plate and stimulated with LPS (100 ng/mL), R848 (5  $\mu$ g/mL), TL8 (100 ng/mL),  
723 ssRNA (1.6  $\mu$ g/mL) + DOTAP (50  $\mu$ g/mL), ssRNA+LL37 complex (as described above), and respective  
724 NET content (1:20 dilution) for 24 h at 37°C and 5% CO<sub>2</sub>. Where indicated, the TLR8 inhibitor CU-  
725 CPT9a was added to the cells at a concentration of 1  $\mu$ M 2h before stimulation and was not removed  
726 for the incubation of the cells with the respective stimuli. After the stimulation, the plate was

727 centrifuged for 5 min at 1500 rpm and the supernatant was collected and stored at -80 °C until the  
728 ELISA was performed.

#### 729 **Preparation of NETs and isolation of naRNA/whole PMN RNA**

730 NETs were prepared by 600 nM PMA treatment for 4 h at 37°C and 5% CO<sub>2</sub>, or cells were left  
731 untreated during the incubation as the mock control. After incubation, the neutrophils were gently  
732 washed three times with PBS to get rid of PMA as the stimulus for NET formation, any cytokines  
733 released by the cells and unstimulated PMNs, as those do not adhere to the uncoated petri dish used  
734 here. In some conditions (as indicated) during the NET preparation process and for storage, naRNA  
735 was protected by addition of 10 U/μL RNase inhibitor (= Mock or PMA NETs + RNase Inhibitor). For  
736 digest of NETs with the respective enzymes, the NET content was incubated for 20 min at 37 °C with  
737 RNase A (Thermo Fisher, EN0531; 100 μg/mL, EDTA for DNase inhibition added) or DNase I (Thermo  
738 Fisher, EN0521) for 60 min at 37 °C (1 U/10 μL, RNase inhibitor for RNase inhibition added). For  
739 isolation of naRNA, RNase inhibitor was added to the PMNs during NET formation. After the above  
740 described washing process, PMA or mock NETs were resuspended in 300 μL of ML buffer and RNA  
741 isolation was performed according to the manufacturer's instructions (NucleoSpin miRNA isolation  
742 kit, Macherey-Nagel, 740971.50). The RNA was eluted in 50 μL RNase/DNase/endotoxin-free H<sub>2</sub>O  
743 and the concentration was determined with a Nanodrop Spectrophotometer. For isolation of whole  
744 PMN RNA, untreated PMNs were directly lysed, and the RNA was isolated from the cells according to  
745 the manufacturer's instructions.

#### 746 **Preparation of human primary stem cell-derived PMNs**

747 Stem cells derived from human healthy donors were prepared and differentiated as described (Sioud  
748 2020). In brief, bone marrow was diluted in PBS, carefully layered on Ficoll-Paque medium (density:  
749 1.077 g/mL) and centrifuged at 500 x g for 25 min at RT without brakes. The interphase layer  
750 containing the mononuclear cell fraction was transferred to a new tube and washed twice with 30  
751 mL ice-cold PBS by centrifugation at 300 x g for 8 min at 8 °C. Further, the cells were resuspended,  
752 counted, and isolated using Human CD34 MicroBead Kit (Miltenyi) for magnetic beads-based  
753 isolation of CD34<sup>+</sup> cells from BMMNCs. Afterwards, the number of CD34<sup>+</sup> HPSCs was determined and  
754 cultured in CD34<sup>+</sup> culture medium (Stemline II Hematopoietic Stem Cell Expansion medium  
755 supplemented with 10% FCS, 1% L-glutamine, 1% penicillin/streptomycin, and a human recombinant  
756 cytokine cocktail consisting of 20 ng/mL IL-3, 20 ng/ mL IL-6, 20 ng/mL TPO, 50 ng/mL SCF, and 50  
757 ng/mL FLT-3L) at a density of 2 x 10<sup>5</sup>/mL at 37 °C and 5% CO<sub>2</sub>. The medium was replaced every  
758 second day and the cells were cultured for 14 days. During the differentiation process, the cells were  
759 treated with 100 μM 5-ethynyl uridine for 14 days for subsequent click chemistry labeling of  
760 endogenous RNA or were left untreated as negative controls. To verify differentiation, cell  
761 morphology was assessed using Cytospin assay. In brief, the Cytoclip™ slide clips were loaded by  
762 fitting the filter card, the sample chamber, and the glass slide. An assemble Cytoclip™ slide clip was  
763 then placed in the slide clip support plate of the cytospin centrifuge. 2 x 10<sup>4</sup> cells from liquid culture  
764 differentiation were pipetted into Cytofunnel™ and centrifuged for 3 min at 200 x g. The cytospin  
765 slides were stained for 5 min in May-Grünwald stain, rinsed shortly with ddH<sub>2</sub>O, and then stained for  
766 10 min in Wright-Giemsa stain. Afterwards, the slides were rinsed shortly with ddH<sub>2</sub>O and cell  
767 morphology was determined using a microscope. To further verify differentiation, flow cytometric  
768 analysis was performed using antibodies specific for the following hematopoietic/myeloid markers:  
769 CD45 (leukocyte marker), CD34 (HSPC marker), CD33 (promyelocyte marker), CD11b (myeloid cell  
770 marker), CD14 (monocyte marker), and CD15 and CD16 (neutrophil markers). Neutrophil percentage  
771 was determined by gating on neutrophils as follows: CD45<sup>+</sup>CD11b<sup>+</sup>CD15<sup>+</sup>, or CD45<sup>+</sup>CD11b<sup>+</sup>CD16<sup>+</sup>, or  
772 CD45<sup>+</sup>CD15<sup>+</sup>CD16<sup>+</sup> cells

#### 773 **BlaER1 cell culture, transdifferentiation and stimulation**

774 BlaER1 cells (WT, *Unc93b*<sup>-/-</sup> and *Tlr8*<sup>-/-</sup>), a kind gift of Holger Heine, Borstel, Germany (Vierbuchen,  
775 Bang et al. 2017), were cultured, transdifferentiated, and stimulated for 18 h with the respective  
776 stimuli as described (Herster, Bittner et al. 2020). In brief, 1x10<sup>6</sup> cells/well were seeded in a 6-well

777 plate and differentiated with 10 ng/mL hIL-3, 10 ng/mL hMCSF and 150 nM  $\beta$ -estradiol in complete  
778 RPMI-1640 (PANBiotech, P04-18525) for 7 days. Afterwards  $5 \times 10^4$  differentiated cells were  
779 reseeded in a 96-well plate, followed by 1 h resting. Cells were treated with the respective stimuli  
780 (LPS at 0.1  $\mu$ g/mL, R848 at 5  $\mu$ g/mL, the TLR8 agonist TL8 at 100 ng/mL or ssRNA+LL37 complex as  
781 described above) and Mock or PMA NETs with or without RNase inhibitor) in complete medium in a  
782 total volume of 125  $\mu$ L/well for 18 h. After stimulation, the cells were centrifuged for 5 min at 1200  
783 rpm, the supernatant was transferred into a new plate and stored at  $-80^\circ\text{C}$  until the ELISA was  
784 performed.

#### 785 **THP-1 cell culture, differentiation and stimulation**

786 THP-1 cells (THP-1 cells were a kind gift from Thomas Zillinger, Bonn, Germany (Coch, Hommertgen  
787 et al. 2019), were cultured in complete RPMI-1640 (Sigma, R8758-24X500ML) medium. For  
788 differentiation into macrophage-like cells,  $5 \times 10^4$  cells/well were seeded in a 96-well plate, treated  
789 with 300 ng/mL PMA and incubated for 16 h at  $37^\circ\text{C}$  and 5%  $\text{CO}_2$ . The next day, the cells were  
790 washed three times with PBS and fresh medium was added, followed by 48 h of resting.  
791 Subsequently, the medium was removed, exchanged by medium containing 200 U/mL IFN- $\gamma$  (Sigma,  
792 I-3265), and the cells were incubated for 6 h. After repeated washing and medium exchange, cells  
793 were treated with the respective stimuli (PMA (25  $\mu$ g/mL) + Ionomycin (0.375  $\mu$ g/mL), LPS (0.1  
794  $\mu$ g/mL), R848 (5  $\mu$ g/mL), TL8 (40 ng/mL), ssRNA+LL37 complex (as described above), Mock NETs +  
795 RNase inhibitor (1:50 dilution), PMA NETs (1:50 dilution) and PMA NETs + RNase inhibitor (1:50  
796 dilution)) in complete medium in a total volume of 125  $\mu$ L/well for 18 h. After stimulation, the cells  
797 were centrifuged for 5 min at 1200 rpm, the supernatant was transferred into a new plate and stored  
798 at  $-80^\circ\text{C}$  until the ELISA was performed.

#### 799 **N/TERT-1 keratinocyte cell culture and stimulation**

800 N/TERT-1 cells (a kind gift from Prof. James Rheinwald (Dickson, Hahn et al. 2000)) were cultured for  
801 less than ten passages in complete CnT-07 medium (CELLnTEC, CnT-07). Two days prior to  
802 stimulation, a total amount of  $2 \times 10^4$  cells/well were seeded in a 96-well plate and incubated at  $37^\circ\text{C}$   
803 and 5%  $\text{CO}_2$ . The medium was renewed, and the cells were stimulated in a total volume of 125  
804  $\mu$ L/well of the respective stimuli diluted in medium (PMA (25  $\mu$ g/mL) + Ionomycin (0.375  $\mu$ g/mL), TL8  
805 (200 ng/mL), ssRNA+LL37 complex (as previously described), as well as Mock and PMA NETs with and  
806 without RNase inhibitor at indicated dilutions). After 24 h stimulation, the cells were centrifuged at  
807 1200 rpm for 5 min and the supernatant was stored in a new plate at  $-80^\circ\text{C}$  until further usage.

#### 808 **Primary normal human epidermal keratinocyte (NHEK) cell culture and stimulation**

809 NHEK cells (Normal Human Epidermal Keratinocytes (NHEK) single juvenile donor, proliferating,  
810 PromoCell, C-12002) were grown and stimulated in Keratinocyte Growth Medium 2 (PromoCell, C-  
811 20111). Two days prior to stimulation, a total amount of  $2 \times 10^4$  cells/well were seeded in a 96-well  
812 plate and incubated at  $37^\circ\text{C}$  and 5%  $\text{CO}_2$ . For stimulation, the medium was renewed with basal  
813 medium (PromoCell, C-20211) containing 1.7 mM  $\text{CaCl}_2$  (Roth, CN93.1) and stimuli were added and  
814 diluted in medium in a final volume of 125  $\mu$ L (R848 (20  $\mu$ g/mL), TL8 (200 ng/mL), ssRNA+LL37  
815 complex, as well as Mock NETs + RNase inhibitor (1:25 dilution) and PMA NETs with and without  
816 RNase inhibitor (1:25 dilution). After 24 h stimulation, the cells were centrifuged at 1200 rpm for 5  
817 min and the supernatant was stored in a new plate at  $-80^\circ\text{C}$  until further usage.

#### 818 **Preparation of 3D human skin equivalent**

819 The 3D human skin equivalent was prepared as described (Bitschar, Staudenmaier et al. 2020).  
820 Briefly, primary fibroblasts were seeded on collagen and incubated in FF medium for five days.  
821 Subsequently, primary keratinocytes were added to the wells and airlifting was performed on day 12.  
822 On day 22, the 3D skin model was stimulated with NET content (25  $\mu$ L/well for one 3D construct  
823 grown in a 12-well chamber) or respective water control for 24 h. Afterwards, supernatant was  
824 harvested for ELISA, RNA was isolated for qPCR analysis and H&E staining was performed.

#### 825 **NK-92 MI cell culture and stimulation**

826 NK-92 MI cells (kindly provided by Melanie Märklin, University Hospital Tübingen) were cultured in  
827 IMDM-Medium (Lonza, 12-722F). For stimulation, a total amount of  $1 \times 10^5$  cells/well were seeded in  
828 a volume of 200  $\mu\text{L}$  and rested for 2 h at  $37^\circ\text{C}$  and 5%  $\text{CO}_2$ . The cells were stimulated with LPS (100  
829 ng/mL), CpG (2.5  $\mu\text{M}$ ) + DOTAP (25  $\mu\text{g/mL}$ ), R848 (5  $\mu\text{g/mL}$ ), TL8 (100 ng/mL), ssRNA (1.6  $\mu\text{g/mL}$ ) +  
830 DOTAP (50  $\mu\text{g/mL}$ ), ssRNA+LL37 complex (as described above), or NET content (1:100 dilution) for 24  
831 h and afterwards centrifuged for 5 min at 1500 rpm. Subsequently, the supernatant was transferred  
832 into a new plate and stored at  $-80^\circ\text{C}$  until further usage.

### 833 Flow cytometry

834 After PMN isolation, the purity and activation status of the cells was determined by flow cytometry  
835 as described (Herster, Bittner et al. 2020). In brief, 200  $\mu\text{L}$  of cells were transferred into a 96-well  
836 plate (U-bottom) and centrifuged for 5 min at  $448 \times g$ . Afterwards, blocking was performed using  
837 pooled human serum diluted 1:10 in PBS for 15 min at  $4^\circ\text{C}$ . After washing, the samples were  
838 stained for 20 min at RT in the dark and fixed (4% PFA in PBS) after repeated washing for 10 min  
839 at RT in the dark. After an additional washing step, the cell pellets were resuspended in 300  $\mu\text{L}$  PBS and  
840 measurements were performed on a FACS Canto II (BD Bioscience, Diva software). Analysis was  
841 performed using FlowJo V10 analysis software.

### 842 RNA sequencing analysis of naRNA

843 Isolated naRNA was analyzed for quality control using the Agilent 4200 TapeStation system.  
844 Subsequently, the RNA was sequenced according to NEBNext® Ultra™ II Directional RNA Library Prep  
845 Kit for Illumina® using the protocol for use with rRNA Depleted FFPE RNA. The data was quantified  
846 using Salmon Version 1.5.0 and tximport was used to obtain the transcript-level quantification. For  
847 transcript classification, GENECODE annotation was performed.

### 848 Fluorescence microscopy of fixed human or murine primary neutrophils

849 500  $\mu\text{L}$  of  $1.6 \times 10^6$  cells/mL of human blood PMNs, and  $2 \times 10^6$  cells/mL murine BM-PMNs were  
850 seeded in a 24-well plate containing poly-L-lysine-coated glass coverslips (Electron Microscopy  
851 Sciences, 72292-04) and rested for 30 min before stimulation at  $37^\circ\text{C}$  and 5%  $\text{CO}_2$  with the according  
852 stimuli (as described above) for 3 h (human) or 16 h (murine), respectively, as adapted from  
853 Brinkmann *et al.*, 2004 (Brinkmann, Reichard et al. 2004). After stimulation, the cells were carefully  
854 washed with PBS and fixed with fixation buffer (Biolegend, 420801) for 10 min at RT in the dark.  
855 Afterwards, the cells were blocked with PBS containing 0.1 % heat-inactivated diethylpyrocarbonate  
856 (DEPC) (Roth, K028.2), 10 % chicken serum (Normal Chicken Serum Blocking Solution S-3000,  
857 Biozol/Vectorlabs, VEC-S-3000-20), 0.1 % saponin (Applichem, A4518.0100), as well as 10 U/ $\mu\text{L}$  RNase  
858 inhibitor for 2 h at RT. The primary antibodies (rRNA Y10b, hLL37, see Supplementary Table S3) were  
859 diluted 1:50 in blocking buffer and subsequently incubated for 2 h at RT. Afterwards, the cells were  
860 washed three times with PBS containing 0.1 % heat-inactivated DEPC and incubated with the  
861 secondary antibodies (see Supplementary Table S3) in a 1:500 dilution in blocking buffer for 1 h.  
862 After repeated washing, the cells were incubated with Hoechst 33342 (Thermo Fisher; 1  $\mu\text{g/mL}$ ) for 5  
863 min to stain nuclear DNA. Secondary antibodies alone did not yield any significant staining under  
864 identical staining and acquisition conditions. The coverslips were mounted (ProLong™ Diamond  
865 Antifade Mountant, Thermo Fisher, P36961) on glass slides and left to dry overnight at RT in the dark.  
866 Subsequently, the samples were stored at  $4^\circ\text{C}$  before microscopy using a Zeiss LSM800 Confocal  
867 microscope (40x or 63x magnification with Z-stack acquisition, AiryScan mode) and image analysis  
868 using ImageJ-Win64 and Zen Blue3 software was performed.

### 869 Quantification of NET formation

870 To quantify the formation of NETs, microscopy images were obtained using a Zeiss LSM800 Confocal  
871 microscope with a 40x objective and 3x3 tiles acquisition. Three images per sample of three  
872 biological replicates were taken. To quantify NET formation by using NET-related signal dispersion of  
873 rRNA and DNA signal, ImageJ software was used, and a threshold (Triangle threshold) was applied as  
874 originally described (Zack, Rogers et al. 1977). Particles were analyzed with a ROI (region of interest)



875 manager (size (micron<sup>2</sup>): 100-infinity (pixel units); circularity 0.00-1.00) and average size and number  
876 of particles (ROIs) were assessed. In NETs, RNA and DNA signals showed up in a greater number and  
877 smaller size, making the usage of the ratio suitable as a measurement of NET-related signal  
878 dispersion. In the case of using the DNA signal only to assess NET formation, ImageJ software was  
879 used to create a PNG image and a grid with 8x8 tiles was manually applied to the images. Tiles  
880 containing extracellular DNA structures were manually counted in a blinded manner as NET-positive  
881 tiles.

#### 882 **Live fluorescence microscopy of enzymatic digest of human NETs**

883 500  $\mu$ L of  $1.6 \times 10^6$  cells/mL of human blood PMNs were seeded in a 4-well glass bottom microscopy  
884 cell culture dish (Greiner, 627871) and rested for 30 min before stimulation at 37°C and 5% CO<sub>2</sub> with  
885 PMA (600 nM) for 3 h. After stimulation, the medium was carefully removed and the cells were  
886 washed with PBS before adding fresh culture medium (RPMI culture medium without phenol red  
887 (Sigma-Aldrich, R7509) + 10% FBS (heat inactivated, sterile filtered, TH Geyer, 11682258)). Hoechst  
888 33342 (Thermo Fisher, 1  $\mu$ g/mL) to stain nuclear DNA and SYTO RNaselect Green fluorescent dye  
889 (Thermo Fisher, 50  $\mu$ M) to stain rRNA was added to the cells, as well as RNase A (Thermo Fisher,  
890 EN0531; 100  $\mu$ g/mL) or DNase I (Thermo Fisher, EN0521, 1 U/10  $\mu$ L) was added between time point 0  
891 and 5 min. Live cell imaging was performed using a Zeiss LSM800 Confocal microscope with a 63x  
892 objective and Z-stack acquisition, taking an image every 5 min for 30-60 min respectively. Image  
893 analysis and video creation was performed using ImageJ-Win64.

#### 894 **Click chemistry of primary, stem cell-derived PMNs and fluorescence microscopy**

895 500  $\mu$ L of  $1.6 \times 10^6$  cells/ml of human stem cell-derived PMNs treated with 5-ethynyl uridine or left  
896 untreated were seeded in a 24-well plate containing poly-L-lysine-coated glass coverslips and rested  
897 for 30 min before stimulation with PMA (600 nM) at 37°C and 5% CO<sub>2</sub> for 12 h. After stimulation, the  
898 cells were washed and permeabilized with ice-cold acetone (Applichem, A1582.2500PE) 1:1  
899 methanol (Honeywell, 32213-2.5L) for 5 min at RT. Subsequently, the click chemistry (reagents see  
900 Supplementary Table S4) labeling of endogenous RNA was performed as described (Presolski, Hong  
901 et al. 2011). Briefly, in a total volume of 500  $\mu$ L, 2  $\mu$ L of AF546-Azide, a pre-mixture of 1 mM CuSO<sub>4</sub>  
902 and 1.25 mM THPTA, 5 mM aminoguanidine-hydrochloride and 5 mM Na-ascorbate in PBS were  
903 added to the cells in a 24-well plate. The wells were sealed with plastic foil and incubated for 1 h at  
904 RT while shaking in the dark. For negative controls, 5-ethynyl uridine untreated cells incubated with  
905 complete click chemistry reagents and 5-ethynyl uridine treated cells incubated with PBS and AF546-  
906 Azide only were used. No significant signals were observed. After the incubation, the cells were  
907 washed three times for 5 min with PBS and counterstained with rRNA Y10b-AF647 (see  
908 Supplementary Table S3) at 1:50 in PBS for 2 h at RT in the dark. After repeated washing, the cells  
909 were incubated with Hoechst 33342 to stain nuclear DNA and mounted as described above. Imaging  
910 and analysis were performed as previously described.

#### 911 **Electron microscopy**

912 For Electron microscopy, 500  $\mu$ L of  $1.6 \times 10^6$  cells/ml of human blood-derived PMNs were seeded in a  
913 24-well plate containing coverslips which were pre-coated with 0.01 % poly-L-lysine (Sigma, A-005-C)  
914 for 15 min at 37°C. Cells were rested for 30 min at 37°C and 5% CO<sub>2</sub> and subsequently stimulated  
915 with 1200 nM PMA for 3 h. Afterwards, the cells were fixed in 2.5% glutaraldehyde in PBS for 1 h at  
916 room temperature followed by 4°C. Samples were post-fixed with 1% osmium tetroxide for 1 h on  
917 ice. Subsequently, samples were dehydrated in a graded ethanol series followed by critical point  
918 drying (CPD300, Leica Microsystems) with CO<sub>2</sub>. Finally, the cells were sputter-coated with a 4 nm  
919 thick layer of platinum (CCU-010, Safematic) and examined with a field emission scanning electron  
920 microscope (Regulus 8230, Hitachi High Technologies) at an accelerating voltage of 3 kV. For  
921 antibody labeling, cells treated as described above were fixed in 4% formaldehyde in PBS for 1-2  
922 hours at room temperature and 4°C overnight. After washing and blocking (0.2% gelatin in PBS)  
923 samples were incubated for 1 h at room temperature with rRNA Y10b as the primary antibody in  
924 blocking buffer and for 1 h at RT with goat anti-mouse antibodies coupled to 12 nm or 6 nm gold in

925 blocking buffer (Jackson ImmunoResearch, code numbers 115-205-146 and 115-195-166,  
926 respectively). Samples labeled with 6 nm gold were further silver enhanced. Following  
927 immunolabeling, the samples were treated with 1% uranyl acetate for 5 min at RT, dehydrated and  
928 critical point dried as before. Samples were sputter-coated with a 5 nm thick layer of carbon (CCU-  
929 010, Safematic) and analyzed in the SEM with an accelerating voltage of 5 kV.

#### 930 **Transient transfection of HEK293T cells**

931 HEK293T cells were transiently transfected with the respective TLR8, TLR7, TLR9 and NF- $\kappa$ B reporter  
932 plasmids as described (Colak, Leslie et al. 2014) (see Supplementary Table S5 for plasmids) using X-  
933 tremeGENE™ HP DNA Transfection Reagent (Merck, 6366236001). A total amount of  $5 \times 10^4$   
934 cells/well were seeded in a 24-well plate one day prior to transfection. For the transfection of one  
935 well, 100 ng of the according TLR plasmid, 100 ng of the firefly luciferase NF- $\kappa$ B reporter and 10 ng  
936 *Renilla* luciferase control reporter was mixed in Opti-MEM™ Reduced Serum Medium (Thermo  
937 Fisher, 31985062) in a total volume of 50  $\mu$ L. After 15 min incubation at RT, the transfection mix was  
938 added to the cells and the cells were incubated for 48 h. Prior to subsequent stimulation, the  
939 medium was changed to complete DMEM medium (Sigma, D5796-24X500ML), and the cells were  
940 incubated with the respective NET content stimuli and controls (R848 (2.5  $\mu$ g/mL), TL8 (100 ng/mL),  
941 CpG (1.25  $\mu$ M) + DOTAP (25  $\mu$ g/mL), ssRNA (0.6  $\mu$ g/mL) + DOTAP (20  $\mu$ g/mL), Mock NETs + RNase  
942 inhibitor (1:50 dilution), PMA NETs (1:50 dilution), PMA NETs + RNase inhibitor (1:50)) for 18 h at  
943 37°C and 5% CO<sub>2</sub>. Supernatants were then removed, and the cells frozen briefly at -80 °C.  
944 Subsequently they were used for dual luciferase assay.

#### 945 **Dual luciferase reporter assay**

946 The dual luciferase reporter assay for detection NF- $\kappa$ B activation after TLR transfection and  
947 subsequent stimulation was performed as described (Herster, Bittner et al. 2020). In brief,  
948 supernatants were removed from the cells after stimulation and 60  $\mu$ L/well of 1X passive lysis buffer  
949 (E194A, Promega) was added. The plate was then incubated for 15 min at RT on the plate shaker and  
950 subsequently stored at -80°C for at least 15 min to facilitate complete cell lysis. After thawing, the  
951 cell solution (60  $\mu$ L) was transferred into a V-bottom 96-well plate and centrifuged for 10 min at  
952 2500 rpm and 4°C to pellet cell debris. Ten microliters of supernatant were then transferred into a  
953 white microplate and each condition was measured in triplicates using the FLUOstar OPTIMA device  
954 (BMG Labtech). Firefly and *Renilla* luciferase activity were determined using the Promega Dual  
955 luciferase kit. Both enzyme activities were measured for 12.5 s with 24 intervals of 0.5 s,  
956 respectively. The data was analyzed by calculating the ratio of the two measured signals, thereby  
957 normalizing each firefly luciferase signal to its corresponding *Renilla* luciferase signal. The ratios were  
958 represented as the relative light units (RLU) of NF- $\kappa$ B activation.

#### 959 **Extracellular bacterial killing of *S. aureus***

960 The killing assay of *S. aureus* with human PMNs was performed according to Brinkmann *et al.*, 2004  
961 (Brinkmann, Reichard et al. 2004). In brief, PMNs were seeded at a density of  $2 \times 10^6$  cells/mL and  
962 incubated with PMA (600 nM) for 2 h at 37 °C. Afterwards, the medium was carefully replaced with  
963 serum-free culture medium, containing 2% heat-inactivated pooled human serum with cytochalasin  
964 D (10  $\mu$ g/mL) and incubated further for 15 min before infection with bacteria. Cytochalasin D  
965 treatment did not affect NETs and this concentration was effective in blocking bacterial phagocytosis.  
966 To investigate whether naRNA of NETs was important in extracellular killing, samples were either  
967 treated with RNase A (Thermo Fisher, EN0531; 100  $\mu$ g/mL) or DNase I (Thermo Fisher, EN0521; 1  
968 U/10  $\mu$ L) for 2 h during NET formation, or after NET formation during the 30 min bacterial killing  
969 process. Samples were centrifuged at 700 x g for 10 min and incubated at 37 °C and 5% CO<sub>2</sub> for 30  
970 minutes. Bacterial killing was measured as percentages of control values (bacteria incubated alone in  
971 media without neutrophils).

#### 972 **In vivo analysis of naRNA DAMP effects**

973 To investigate the effect of NETs with or without RNase inhibitors and the respective TLR signaling,  
974 20  $\mu\text{L}$  of NET content and the respective controls were injected into the ears of C57BL/6 and *Tlr13*<sup>-/-</sup>  
975 mice intradermally on day 0. Afterwards, as a measure of inflammation, the ear thickness was  
976 assessed using a manual caliper (0.01–10 mm, Peacock, Tokyo, Japan) until day 4.

#### 977 **Neutrophil infiltration *in vivo* fluorescence imaging**

978 The *in vivo* experiment for investigating neutrophil infiltration was performed as described (Herster,  
979 Bittner et al. 2020). Briefly, LysM<sup>EGFP/+</sup> mice were injected intradermally with 20  $\mu\text{L}$  of PMA or Mock  
980 NET content or respective controls. LysM<sup>EGFP/+</sup> mice were then anesthetized with inhalation isoflurane  
981 and *in vivo* fluorescence imaging was performed using the IVIS Lumina II imaging system (Caliper).  
982 EGFP fluorescence was measured using excitation (465 nm), emission (515–575 nm), and exposure  
983 time (0.5 s). Data are quantified as total radiant efficiency ([photons/s]/[ $\mu\text{W}/\text{cm}^2$ ]) within a circular  
984 region of interest using Living Image software (Caliper).

#### 985 **Imiquimod model of psoriatic skin inflammation**

986 To analyze the effect of RNA signaling in an *in vivo* model for psoriasis, the well-established  
987 imiquimod mouse model was used (Gilliet, Conrad et al. 2004). C57BL/6 and *Tlr13*<sup>-/-</sup> mice were used  
988 and, briefly, 70  $\mu\text{L}$  (62.5 mg) of imiquimod (5%, Taro Pharmaceuticals Industries, Hawthorne, NY) was  
989 applied daily to both sides of a mouse ear for 5 consecutive days (day 0 to 4). Ear thickness was  
990 measured with a manual caliper (0.01–10 mm, Peacock, Tokyo, Japan) before imiquimod application.  
991 A day after the last application of imiquimod (day 5), full-thickness ear skin was excised with surgical  
992 scissors for histologic analysis.

#### 993 **ELISA**

994 To measure cytokine release of BlaER-1, THP-1, N/TERT-1, NHEK, NK-92 MI, PBMCs and 3D human  
995 skin equivalent after stimulation with NET content and respective controls, ELISA Kits for hIL-8 (ELISA  
996 MAX™ Deluxe Set Human IL-8, Biolegend, 431504), hIL-6 (ELISA MAX™ Deluxe Set Human IL-6,  
997 Biolegend, 430504), IFN- $\gamma$  (ELISA MAX™ Deluxe Set Human IFN- $\gamma$ , Biolegend, 430104), and TNF (TNF  
998 alpha Human Uncoated ELISA Kit, Invitrogen, 88-7346-88) were used according to the manufacturer's  
999 instructions. Samples were assessed in triplicates.

#### 1000 **qPCR analysis of IL-8 expression of 3D human skin equivalent**

1001 To investigate IL-8 expression of 3D human skin equivalent after stimulation with NET contents, qPCR  
1002 analysis was performed. First, total RNA was isolated using the RNeasy Mini Kit (Qiagen, 74106) for  
1003 animal tissues and cells. For cDNA preparation, the High-Capacity RNA-to-cDNA-Kit (Thermo Fisher,  
1004 4387406) was used according to the manufacturer's instructions. For the qPCR, the TaqMan™ system  
1005 was used. Briefly, a master mix of TaqMan™ Universal Mastermix II (Thermo Fisher, 4440040) and  
1006 TaqMan™ Gene Expression Assay (Thermo Fisher, 4448892) was prepared according to the  
1007 manufacturer's instructions. For one reaction, 5.5  $\mu\text{L}$  master mix and 4.5  $\mu\text{L}$  of the respective cDNA  
1008 (IL-8 and TBP) were mixed and the qPCR was run. Analysis in triplicates was performed using  
1009 QuantStudio Real-Time-PCR software version 1.3 (Thermo Fisher).

1010 **Supplementary Tables**

1011 **Supplementary Table 1: commercial TLR ligands and inhibitors; enzymes**

Component	Company	Product no.
Cl-amidine	Merck	506282
CpG PTO 2006	TIB Molbiol	n/a, see Table S2
CU-CPT9a	Invivogen	inh-cc9a
DNase I	Thermo Fisher	EN0521
DNase inhibitor 50 mM EDTA	Thermo Fisher	EN0521
DOTAP	Roth	L787.2
Ionomycin	Sigma	I0634-1MG
LL37	Invivogen	tlrl-l37
LPS-EK (ultrapure)	Invivogen	tlrl-pekips
Nigericin	Invivogen	tlrl-nig
PMA	Invivogen	tlrl-pma
R848 (Resiquimod)	Invivogen	tlrl-r848
RNase A	Thermo Fisher	EN0531
RNase inhibitor	Promega	N2615
TL8-506	Invivogen	tlrl-tl8506

1012

1013 **Supplementary Table 2: Nucleic acid TLR agonists**

Component	Sequence	Backbone	Company
RNA40	5'GsCsCsGsUsCsUsGsUsUsGsUsGsUsGsAsCsUsC3'	Phosphorothioate	Eurogentec
CpG PTO 2006	5'TsCsGsTsCsGsTsTsTsGsTsCsGsTsTsTsGsTsCsGsTsT3'	Phosphorothioate	TIB

1014

1015 **Supplementary Table 3: Antibodies and conjugation kit**

Item	Fluorophore	Species	Isotype	Company	Product no.
Anti-hLL37	DyLight 550	Rabbit	IgG	LSBio	LS-B6696-500
DyLight 550 Conjugation Kit (Fast)	DyLight 550	-	-	Abcam	ab201800

Anti-rRNA (Y10b)	unconjugated	mouse	IgG <sub>2a</sub> κ	Santa Cruz Biotechnology	sc-33678
Anti-rRNA (Y10b) Alexa Fluor® 647	AF647	mouse	IgG <sub>2a</sub> κ	Santa Cruz Biotechnology	sc-33678 AF647
Anti-mouse IgG	AF647	Chicken	IgY	Thermo Fisher	A-21463
Hoechst 33342		-	-	Thermo Fisher	H21492
SYTO RNaselect Green fluorescent dye		-	-	Thermo Fisher	S32703

1016

1017 **Supplementary Table 4: Click chemistry reagents**

Reagent	Company	Product no.
AF546-Azide	Jena Bioscience	CLK-1283-1
Aminoguanidine-Hydrochloride	Merck	396494-25G
CuSO <sub>4</sub> -click chemistry grade	Jena Bioscience	CLK-MI004-50.1
5-Ethynyluridine	Jena Bioscience	CLK-N002-10
Na-Ascorbate-click chemistry grade	Jena Bioscience	CLK-MI005-1G
THPTA (Tris((1-hydroxy-propyl-1H-1,2,3-triazol-4-yl)methyl)amine)	Jena Bioscience	CLK-1010-25

1018

1019

1020 **Supplementary Table 5: Plasmids used for HEK293T transfection**

Plasmid name insert	Vector backbone	Insert
NF- $\kappa$ B reporter	pGL3	6x NF- $\kappa$ B response element
Renilla	pRL-TK	Renilla
hTLR7	pcDNA3.1 (+)	hTLR7
hTLR8	pcDNA3.1 (+)	hTLR8
hTLR9	pSEM-hTLR9	hTLR9

1021

1022 **Supplementary Table 6: primers used for qPCR**

Gene	Assay number
IL-8	Hs00174103_m1
TBP (housekeeper)	HS00427620_m1

1023

1024 **Supplementary Table 7: 10x Ammonium chloride erythrocyte lysis buffer**

Compound	Company	Product no.
1.54 M NH <sub>4</sub> Cl	Roth	5470.1
100 mM KHCO <sub>3</sub>	Fluka	60220
1 mM EDTA; pH 8	Thermo Fisher	15575020
dissolved in Ampuwa water	Fresenius Kabi	1833
pH adjusted to 7.3, sterile filtered (0.22 $\mu$ m)		

1025

